General Disclaimer

One or more of the Following Statements may affect this Document

- This document has been reproduced from the best copy furnished by the organizational source. It is being released in the interest of making available as much information as possible.

- This document may contain data, which exceeds the sheet parameters. It was furnished in this condition by the organizational source and is the best copy available.

- This document may contain tone-on-tone or color graphs, charts and/or pictures, which have been reproduced in black and white.

- This document is paginated as submitted by the original source.

- Portions of this document are not fully legible due to the historical nature of some of the material. However, it is the best reproduction available from the original submission.

(NASA-CR-169283) EXPERIMENTAL STUDY OF TURBULENCE IN BLADE END WALL CORNER REGION (City Coll. Research Foundation) 110 p HC A06/MF A01 CSCL 20D
N82-31639
Unclas
G3/34 28791

EXPERIMENTAL STUDY OF TURBULENCE IN BLADE END WALL CORNER REGION

TECHNICAL REPORT
PREPARED
UNDER NASA GRANT NO.: NAG 3-122

PRINCIPAL INVESTIGATOR: PROFESSOR R. RAJ
NASA TECHNICAL OFFICER: DR. D.R. BOLDMAN
DATE OF REPORT: AUGUST, 1982

TURBOMACHINERY LABORATORY
DEPARTMENT OF MECHANICAL ENGINEERING
THE CITY COLLEGE OF NEW YORK
NEW YORK, N.Y. 10031

EXPERIMENTAL STUDY OF TURBULENCE IN BLADE END WALL CORNER REGION

TECHNICAL REPORT
PREPARED
UNDER NASA GRANT NO.: NAG 3-122

PRINCIPAL INVESTIGATOR: PROFESSOR R. RAJ
NASA TECHNICAL OFFICER: DR. D.R. BOLDMAN
DATE OF REPORT: AUGUST, 1982

TURBOMACHINERY LABORATORY
DEPARTMENT OF MECHANICAL ENGINEERING
THE CITY COLLEGE OF NEW YORK
NEW YORK, N.Y. 10031

TABLE OF CONTENTS

SUMMARY

In this report are presented the detailed literature search on corner flows and wall pressure fluctuations, design and fabrication of the test model, preliminary results on boundary layer, flow visualization, turbulence intensity and spectra measurements. Also presented are the design considerations and fabrication report on the newly built wind tunnel to be used for subsequent continuation of the research effort on this project.

I. LITERATURE REVIEW ON CORNER FLOWS

The literature review on corner flows can be carried out in two parts, laminar and turbulent corner flows. Each of these can be further subdivided into several cases. Two cases of practical importance to turbomachinery component configurations are:

(a) When boundary layer development starts at the same time on both the bodies and

(i) the surfaces of both of the bodies are uncambered

(ii) One of the body surfaces is uncambered and the second is cambered.

(b) When boundary layer developed on one of the bodies is intercepted by the second body and:

(i) the surfaces of both of the bodies are uncambered

(ii) The body with initial boundary layer is uncambered and the intercepting body is cambered.

These two cases of interest are schematically shown in Fig. 1 (a,b)

1.1 Physical Characteristics of Corner Flows

In case (a) when both the shear layers start at the same time, as in the case of flow through ducts, in the initial laminar portion, the isovels (line joining equal velocity points) bulge away from the corner as shown in Fig. 2(a). However, after the shear layer becomes turbulent, the bulge turns toward the corner. When the flow is laminar, the production of the streamwise component of vorticity, which gives rise to the secondary flow, is due to stretching of the vorticity vector and skewing of the mean shear by action of a transverse pressure gradient or body forces. Prandtl called it the Secondary Flow of the First Kind.

When the flow becomes turbulent, the time averaged action of anisotropic, inhomogeneous turbulence transports the vorticity, and the resultant orientation gives rise to a streamwise component. This is called the Secondary Flow of the Second Kind.

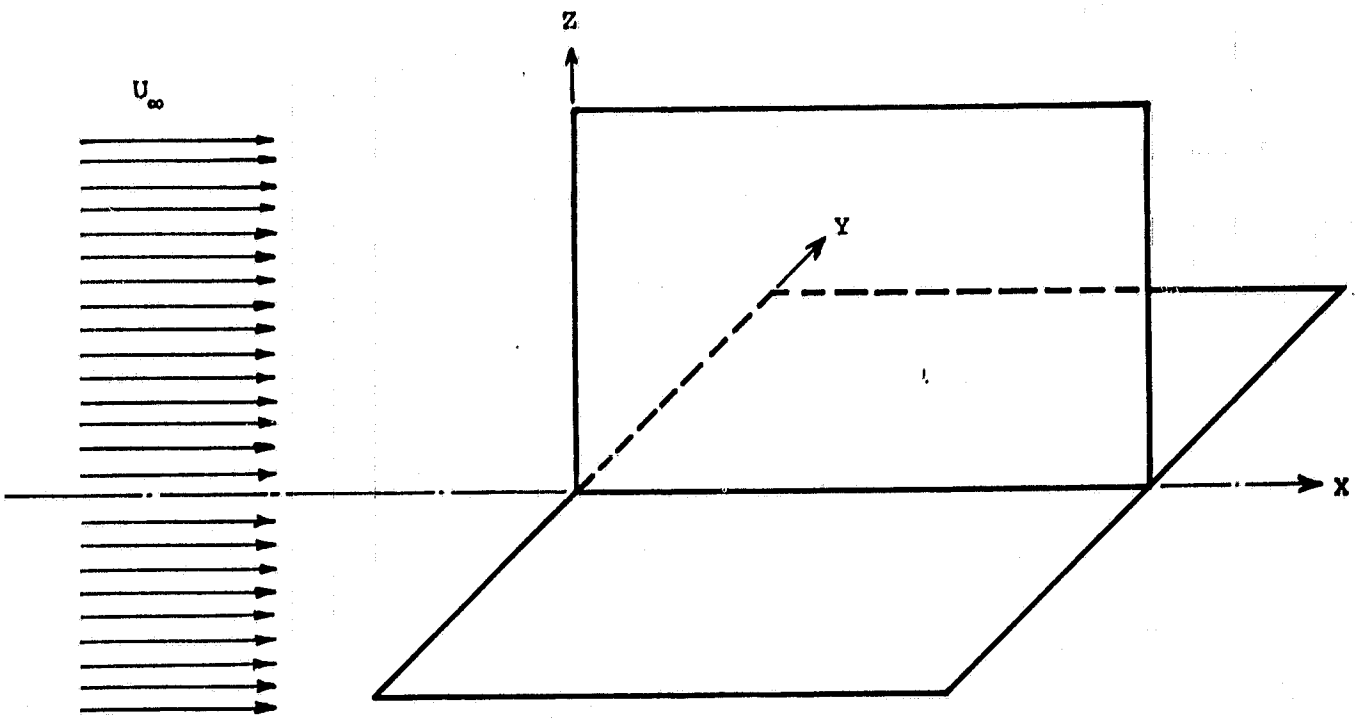

(a)

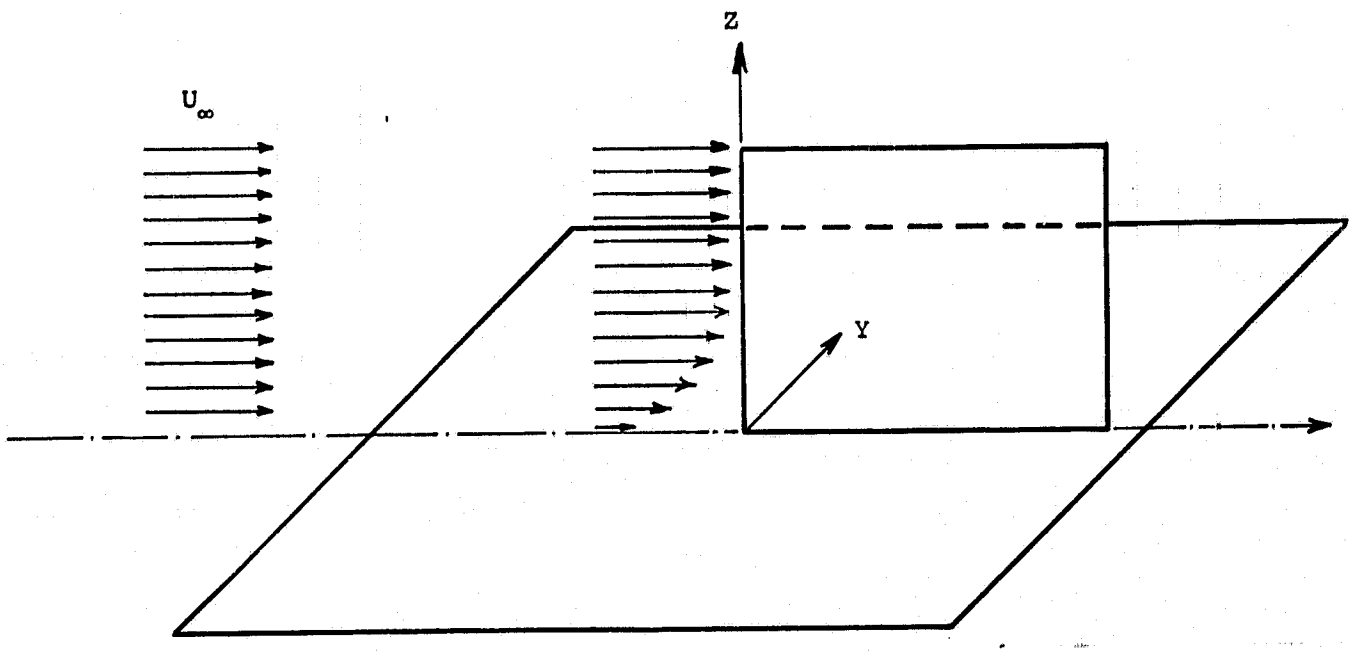

(b)

Figure 1. Configurations for Possible Types of Corner Flows

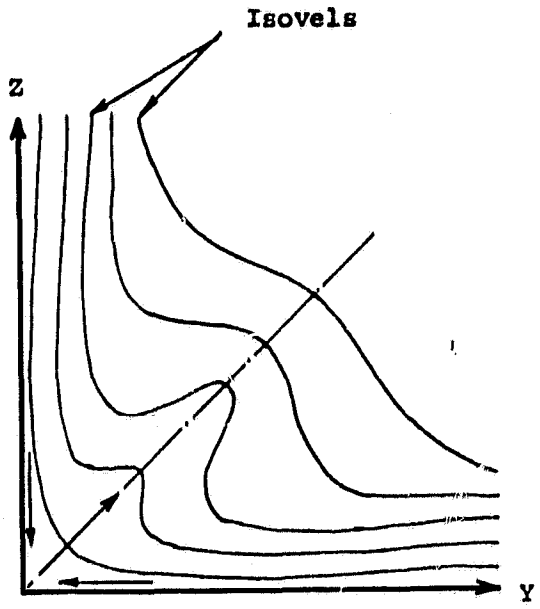

(a) Laminar

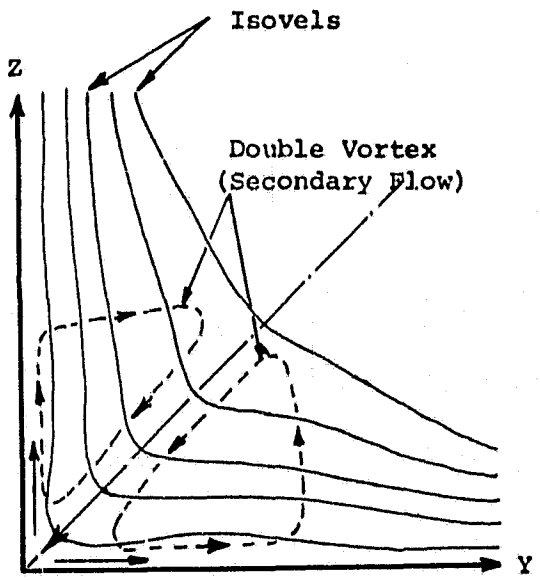

(b) Turbulent

Figure 2. Shapes of Isovels in Laminar and Turbulent Corner Flows

In case (b), Secondary Flow of the First Kind is predominant. The vortex sheet in the boundary layer of the first body is skewed by the presence of the second body, which gives rise to a "horse shoe" vortex. Downstream, along the corner, the turbulent stresses dissipate the strength of this "horse shoe" vortex and inside this envelope Seconday Flow of the Second Kind starts forming. The shape of the "horse shoe" vortex is strongly dependent on the shape of the leading edge of the body obstructing this flow.

Isovels of case (a) and the secondary flow directions of case (b) are shown in Fig. 2 (a,b) and Fig. 3 (a,b), respectively. These figures are qualitative representations. Depending on streamwise curvature of the surfaces and roughness of the surfaces, there will be asymmetry in the isovels and secondary flow. Fig. 2 (a,b) and Fig. 3 (a,b) refer to Fig. 1 (a) and Fig. 1 (b), respectively.

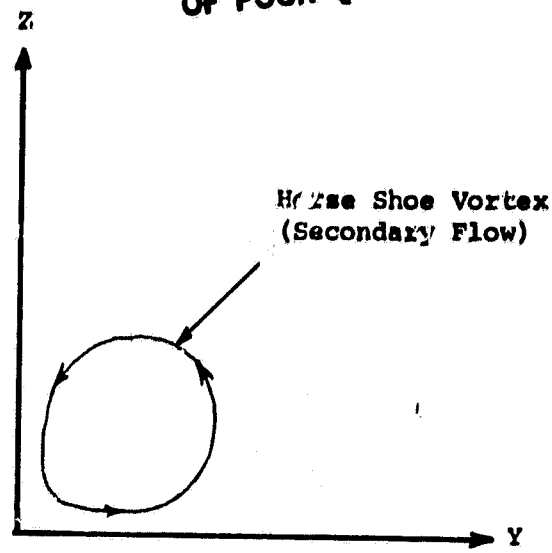

(a) Near Leading Edge

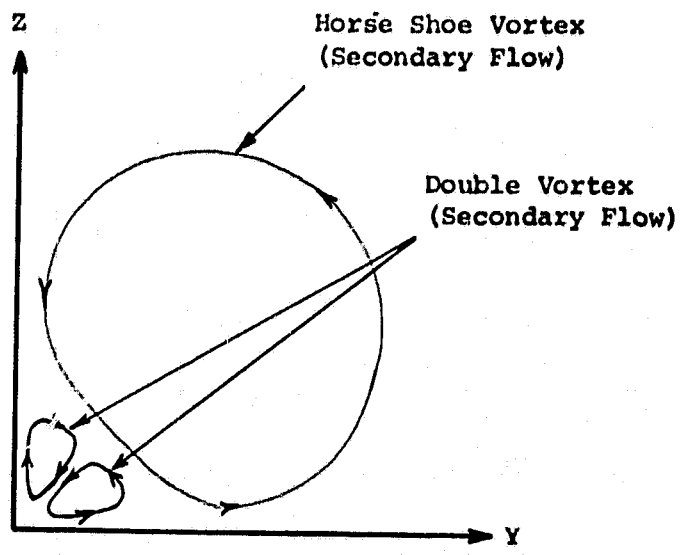

(b) Far Downstream

Figure 3. Development of Horse Shoe Vortex

1.2 Boundary Layer Development Starts at the Same Time on Both the Bodies

1.2.1 Laminar Corner Flows

1.2.1.1 Theoretical Analysis

The problem of laminar flow in streamwise corners was first studied theoretically by Carrier [1]. He considered the change in Blasius solution due to the presence of the perpendicular wall and solved the streamwise momentum and continuity equations. His analysis was incomplete since he neglected the effect of the streamwise vorticity. Dowell [2] tried to estimate the error in the velocity prediction in the direction of edge by linearizing the boundary layer equations given by Carrier, however, only a minor modification was made Pearson [3] introduced the effect of streamwise vorticity in his formulation of the problem. Rubin [4] assumed two potential functions, instead of one as done by Carrier [1], to solve the differential equations. Rubin's [4] analysis showed that several distinct regions can be defined and the equations governing the various

motions can be coupled through asymptotic boundary conditions. Pal and Rubin [5] and Rubin and Grossman [6] developed the numerical technique to solve these equations. The existence of secondary flows towards the corner was demonstrated by these analyses. These analyses also made it possible to define boundary conditions for a limited region in the corner. In the numerical calculations Rubin and Grossman [6], using the above boundary conditions and the Gauss Seidel method of successive iteration solved the equations.

A new approach of using curvilinear coordinate system was devised by Zamir [7,8,9]. His results showed that the streamwise pressure gradient has a great effect on the sign and magnitude of the secondary flow. Zamir used a velocity distribution of the form $U = Ax^n$ in the plane of symmetry, and found that the direction of the secondary flow on the plane of symmetry depends on the exponent "n".

Ghia and Davis [10] obtained a numerical solution for first higher order potential flow. For incompressible potential flow, the displacement effect in the corner is assumed to be the superposition of the displacement effects of the two intersecting semi-infinite plates forming the corner. Ghia

and Davis [10], Ghia [11], and Patel and Goglia [12] used the alternating direction implicit method in solving the governing equations of the incompressible laminar boundary flow in axial corners. For large values of axial distances, Patel and Goglia [12] found good agreement with the results by Rubin and Grossman [6]. Ghia's [11] results did not show the bulge as predicted by Zamir [7,8,9] and found by Zamir and Young [13].

1.2.1.2 Experimental Investigations

Compared to the theoretical effort, little experimental effort has been made on the subject because of the difficulties involved in getting a thick laminar corner layer where useful measurements could be made. Zamir [7] and Zamir and Young [13] made detailed measurements in laminar flow along a 90^{o} corner. The leading edges were streamlined similar to the front half of airfoils and measurements were taken with total pressure and a hot wire anemometer at $Re < 6 \times 10^{4}$. Their measurements showed that the isovels bulge away from the corner in laminar flow which is contrary to that in turbulent flow. They also found a progressive distortion in the velocity profiles with the distance from the leading edge. Barclay [14,15] studied the laminar flow

along a 135^0 corner and found that the effects are much smaller than that along a 90^0 corner and that the distortions are damped along the downstream distance, contrary to the findings of Zamir and Young [13]. This difference is supposedly due to the difference in leading edge shape (a sharper leading edge was used by Barclay) in the two cases. The analytical solution of Carrier [1] seemed to give a good representation of the flow along a 135^0 corner.

El-Gamal [16] and El-Gamal and Barclay [17] studied the flow near a rectangular corner with sharp leading edges. The pressure gradient along the corner was zero or slightly favorable. The profile distortion of the type noted by Zamir and Young [13] was completely absent in their result. This difference again was attributed to the difference in the shape of the leading edge of the corners.

1.2.2 Turbulent Corner Flows

1.2.2.1 Theoretical Analysis

Many investigators used the integral method of calculation for predicting the behavior of flow near the corner. Ligget, et al [18] and Toan [19] were successful in getting the bulge in the isovels by the integral method of calculations. Bragg's [20,21] method of modified law of the wall met with very little success in the flow very near the corner. An "interference" momentum integral equation, to allow for the presence of the second wall by Gersten [22], Bragg [20] and Perkins [23] also did not succeed completely.

The mixing length and eddy viscosity models, tried by Ibragimov et al [24], Gerard [25] and Klinksiek [26] could not predict the value of $\overline{v^2}$, $\overline{w^2}$, $\overline{vw}$. The numerical solutions, based on the model suggested by Launder and Ying [27], provided good agreement for isovel patterns and secondary flow streamlines but provided too small values for the kinetic energy and $(\overline{v^2} - \overline{w^2})$. Gessner and Emery [28,29], Gessner and Po [30] did extensive work on Reynolds stress model relating all the six components to mean rates of strain to give global mixing length representation. However, they failed to predict $(\overline{v^2} - \overline{w^2})$ correctly.

Reynolds stress model similar to Launder and Ying [27], but modelled by means of transport equations was used by Naot et al [31]. This modeling obtained better agreement for $(\overline{v^2} - \overline{w^2})$, but it over-emphasized distortion of the isovels. The transport equations of ε and q^2, were used by Tatchell [32], in a modified model of Launder and Ying [27] for analyzing fully developed flow in a square duct. The model did not provide good agreement near the wall.

Mikhail and Ghia [33] analyzed the effect of compressibility and turbulence using two layer eddy viscosity model as used by Cebeci [34]. Gessner and Emery's [29] algebraic model was modified to cover the entire corner region instead of asymptotic corner region alone. Results obtained by Mikhail and Ghia [33] do not agree too well with Shafir and Rubin [35].

1.2.2.2 Experimental Investigations

Many investigators have reported the nature of secondary flow and the bulge in the isovels towards the corner. However, Rodet [36] was the first to measure the Reynolds stress tensor. Perkins [23] has shown that Rodets measurements were not very reliable due to poor accuracy. Because of the same reason Brundretts [37] measurements in square and rectangular ducts are unreliable.

The preliminary study of turbulence characteristics by Gessner and Jones [38] shows that free stream turbulence does not effect the isovel patterns. Launder and Ying [27] showed that the secondary velocities normalized by friction velocities for different roughness ducts have the same profiles.

The measurements made by Letheusser [39] and Ahmed and Brundrett [40] show that wall shear stress in the vicinity of the corner falls rapidly to zero for square and rectangular ducts and is nearly uniform around the duct perimeter.

Mojola and Young [41] and Mojola [42] reported the results of experiments on developing flow in unbounded 90^{o} corners under zero and adverse pressure gradients. The wall shear stress shows a peak near the corner and rapidly falls to zero at the corner. The turbulent boundary layer was found to be more stable than the laminar one from these measurements.

1.3 Boundary Layer Developed on One of the Bodies is Intercepted by the Second Body

This class of corner flow is dominated by skew induced secondary flow (Secondary flow of the First Kind). Due to the complexity of the problem, very little theoretical study has been done on this type of flow. The studies on this type of flow is further subdivided into two groups.

(i) A cascade of bodies (blades/vanes) intercepting the incoming boundary layer as occurs in turbomachines (called end wall boundary layer flow).

(ii) Only one body is intercepting the incoming boundary layer or the effect due to the adjacent bodies (blade/vane) in the cascade are negligible (called wing body junctions).

1.3.1 Cascade of Bodies Intercepting The Incoming Boundary Layer

Hertzig et al [43] by flow visualization experiments, showed the complexity of this type of flow. The three-dimensional deflection of end wall boundary layer resulted in passage vortices along with the "horse shoe" vortex due to the leading edge shape. Armstrong [44,45] reported a higher order of loss

and Turner [46] showed that boundary layer suction reduced the loss but that there was no change in the flow pattern. Senoo's [47] study showed that the effect of the wall boundary layer depends on the cascade geometry. Recent work on the total pressure distribution at the inlet and outlet are mainly due to Came [48] and Carrick [49].

Prumper [50] and Belik [51] showed the presence of the "horse shoe" vortex and separation ahead of the leading edge due to the "horse shoe" vortex. Owczarek [52] and Owczarek et al [53] discussed the side wall boundary layer migration and accumulation in the corner and presented a model for the roll up passage vortex and effect of Reynolds number on it.

Dring [54] presented a momentum integral analysis for turbine endwall boundary layer. The solution provides the distribution of bounday layer thickness and skewing over the endwall and total pressure deficit of the flow leaving the endwall at the suction surface.

Studies by Sjolander [55] and Langston et al [56] experimentally demonstrated the importance of the "horse shoe" vortex in turbine cascades. One leg of the vortex encounters the suction surface at the point of initiation of the passage ortex. Bradshaw et al [57] considered that it was due to the thick leading edge of the blades used. IN the case of slender

blades the "horse shoe" leg will move only part way across the passage. Marchal and Siverding [58] confirmed the results of Sjolander and Langston. They concluded that the "horse shoe" vortex and its associated phenomenon are more significant in turbines than in compressors.

Penkėn [59] investigated the effect of sharp corners on secondary flows and suggested that rounding of these corners will reduce losses. Investigations by Lakshminarayana et al [60,61] were carried out near the tip of compressor blade and included the effect of tip clearance and scrapping vortex along with the interaction of wall boundary layer and the blades. Unless the amount of loss contributed by these are determined along with their interaction, it is not possible to find the effect of corner flow alone.

1.3.2 Only One Body is Intercepting the Incoming Boundary Layer

The study of flow at the junction of a flat plate and a cylinder was extended to a symmetrical airfoil at zero incidence, for the first time by Vasant Ram [62]. East and Hoxey [63,64] conducted some flow visualization and pressure measurements near the leading edge of a simplified wing body junction and collected data for improving integral calculation methods.

The investigations conducted by Sepri [65], Chu and Young [66] and Young [67] represents a major part of the investigation carried out on this subject. Flow-visualization studies showed that formation of one or more vortices depend on the Reynolds number. Mean values of the three velocity components along with static pressure were measured using a five tube yaw meter, near the corner. Some of these measurements were checked by using a hot wire probe.

Naranjit [68] investigated the near wake of a simple wing body combination. The total pressure measurements showed that the wing wake merged with the fuselage boundary layer without much distortion. His results show clear evidence of an associated streamwise vortex on both sides of the wake.

Shabaka [69] conducted extensive experimental investigation at the corner of an ideal wing body junction formed by a flat plate and an uncambered and constant thickness wing. He measured the distribution of body wall static pressure and all the shear stresses on both the surfaces along with mean velocity distribution. From his measurements,it was observed that eddy viscosity and mixing length models are not suitable for modelling the flow in wing-body corners, where asymmetrical boundary layers interact. He found that the secondary flow in this case was of the First Kind and there was no evidence of the double-vortex pair. However, he found that the strength of the "horse shoe"

vortex rapidly reduces in the down stream direction due to the diffusion action of the Reynolds stress. The corner secondary flows contributed greatly to the turbulent kinetic energy. Regions of negative shear stresses were found in the corner.

Murray [70] used the technique of successive coordinate transformation involving complex analytic functions to construct a general curvilinear coordinate system for the wing-body combination. Using a numerical technique, he solved the equations to find the distribution of the pressure coefficient over the wing body surface.

From the foregoing review, it is evident that very little basic work is done which will lead us to solve Case b(ii), which is a logical step towards analyzing the flow in turbomachinery. Whatever work is done in this field is developmental research in nature. The theoretical and experimental work done on wing-body junction are all on the simplified wing-body junction, which does not account for a number of parameters associated with the real life case.

One of the most obvious real life problems is streamwise curvature. This is present even if the body is non-lifting type (symmetrical airfoil, elliptical bodies, struts, etc.), due to the thickness distribution in the flow direction. This

will introduce a curvature in the streamline i.e. the streamlines will be skewed giving rise to Secondary Flow of the First Kind, which may be in the same or opposite sense of the "horse shoe" vortex, depending on the type of curvature. The second effect is the pressure variation along the corner due to streamwise curvature. The effect of streamwise pressure gradient will be felt both on skewing of the vortex tubes leading to secondary flow of the First Kind and the effect on turbulence which will lead to the modification of the Secondary Flow of the Second Kind. The effect of streamwise curvature on the turbulence quantities are one order of magnitude higher than the rate of strain introduced by the curvature itself. Due to this, the Secondary Flow of the Second Kind (which leads to the formation of double vortex) may be greatly effected by curvature.

There is need to study these various aspects of the problem associated with streamwise curvature before we try to make any intelligent guess on the amount of loss associated with the presence of the corner.

II LITERATURE REVIEW ON WALL PRESSURE FLUCTUATIONS

Kraichnan [71], through theoretical analysis, found that the primary contribution to the pressure fluctuations in the turbulent boundary layer, is the interaction of the turbulence with the mean shear. He estimated that the magnitude of the root-mean-square pressure fluctuations at the wall were of the order of the wall shear stress. Also, different scale eddies contribute to the wall pressure fluctuations and these eddies have different convection speeds. From flow visualization studies, Willmarth and Wooldridge [72] stated that low frequency, large scale flow disturbances are produced by the combined effects of Taylor-Goertler boundary layer instability and density stratification of the air near the wall. When the density stratified air is accelerated into the test section, vorticity is produced and causes the large scale low frequency wall pressure fluctuations.

Another explanation is provided by Bradshaw and Koh [73]. According to them, contribution to pressure fluctuations is due to:

(i) Square of the rate of strain

(ii) Square of the vorticity

They considered Poisson equation for the pressure (incompressible turbulent flow) which is written as

$$-\frac{1}{\rho}\frac{\partial^2 p}{\partial x_j^2} = \frac{\partial u_i}{\partial x_j}\frac{\partial u_j}{\partial x_i} \qquad (1)$$

In this Eqn, both p and u_i have mean and fluctuating parts. The right hand side of Eqn. (1) is called the forcing function and is divided into two parts as explained earlier. Eqn. (1) can be transformed to Eqn. (2) after some simplification.

$$-\frac{1}{\rho}\frac{\partial^2 p}{\partial x_i^2} = e^2 - \tfrac{1}{2}\omega_i^2 \qquad (2)$$

where e is the strain rate and $_i$ is the vorticity vector. The rate-of-strain contribution comes from near saddle points in the streamline pattern (streamlines approaching a given point from north and south, and leaving it from east to west, as seen by an observer moving with the fluid at the point) and this contribution to the right-hand side of Eqn. (2) is positive. As a result $\partial^2 p/\partial x_i^2$ tends to become negative near the point considered and p tends to be a maximum there. Roughly speaking, the rate-of-strain contribution to the fluctuating pressure results from eddy collisions. On the other hand, the vorticity contribution is negative, implying p tends to be minimum at the point considered and this contribution is as a result of eddy rotation.

If some miniature device is introduced (assuming the pressure fluctuation scale is larger than the effective sensing length) into the stream, it creates and record dynamic stresses which are different from the static pressure fluctuations [74].

Some of the earlier work avoided direct measurement of pressure fluctuations and instead used velocity correlations (obtained with the use of hot-wire measurements) to compute pressure correlations. But this can be done only for isotropic turbulence [75]. Willmarth et al. [72] were the first who did intensive measurements of the pressure fluctuations on the wall beneath a thick turbulent boundary layer by using flush mounted pressure transducers.

Experimental measurements of the wall-pressure fluctuations beneath turbulent boundary layer flows have been reported by many authors [References 76 - 80]. It is pointed out by many investigators that experimental results are affected more by the size of the pressure transducers than other parameters such as vibration of pressure transducer, sound field in the test-section, frequency range, spacing of the transducers and surface roughness.

In a turbulent boundary layer, the pressure field is a random continuous scalar function of space and time. In order to recover statistical properties of the pressure field at a point, knowledge of some average of these properties over a finite surface is not sufficient. The finite size of the transducer , gives rise to many problems. For example, the finite size of a transducer sensing element limits the space resolution of a pressure field associated with a local turbulent flow. A

transducer sensing element of non-zero size can only resolve adequately a spatial distribution of pressure, the length scale of which is greater than the characteristic dimensions of the transducer face. The size of the transducer should be such that the sensing element has sufficiently small area to give a good account of a fine spatial structure.

It was pointed out by Willmarth et al. [72] that the transducer response to pressure fluctuations, whose length scale is of the order of the diameter of the sensitive area of the transducer or greater, will not suffer serious cancellation effects. It was noted that pressure fluctuations of scales for which the half wave length was greater than $\delta/30$, were not seriously affected by the transducer size. The characteristics of one of such transducer are:

Transducer diameter d = 4.140 mm δ = 127 mm

δ^* = 12.496 mm, r/δ^* = 0.166 - Type-lead zirconate transducer, Ref. [72]. Where δ is boundary layer thickness.

Response of the transducer, expressed by its receiver function, decreases as the size of the transducer increases [81]. For a periodic pressure distribution and a circular transducer of radius r, the receiver function is proportional to $4J_1^2(kr)/(kr^2)$,

where J_1 ($\cdot\cdot$) denotes the Bessel function of the first kind. Receiver function depends only on the spatial wave length $\lambda = 2\pi/k$ and on the size and shape of the transducer. Receiver function is independent of λ if $2r \prec \lambda$. The constraint on the transducer size is expressed by the relation [81]:

$$r \leq \delta^* = 0.01738 \quad \frac{\nu R_x}{U_\infty}^{0.861}$$

where ν is kinematic viscosity, U_∞ - free stream velocity

Corcos [82] gave a scheme to correct systematically, experimental measurements of all statistical averages related to the space-time correlation of the pressure. It was found that these corrections were quite large. In fact, in most experiments the fine scale contribution to the pressure signal has been so attenuated by the sensing element as to have escaped detection. Extrapolation from the recorded frequency spectra for the smallest detected scale, properly corrected for transducer resolution, suggest that the contributions which have been overlooked may be an appreciable fraction of the signal. As a consequence, some important experimental quantities such as the fluctuating pressure intensity etc. may have been measured with gross error. It was also noted that the correction factor for the pressure intensity is far from a linear relationship with transducer size, so that extrapolation of pressure intensity from results obtained with inadequate transducer size are

likely to be misleading. He pointed out that the transducer size used by Willmarth [72] was still large because they could not resolve a large fraction of the total pressure signal.

The effect of various parameters on pressure fluctuations measurement is briefly given below:

(a) Effect of transducer size:

It was observed [76] that when the size of pressure transducer was quite large compared to boundary layer thickness, it caused attenuation of the pressure signals at high frequencies due to the cancellation of small-scale components of the pressure field over the face of the transducer. As a result, small-scale fluctuations could not be analyzed or measured accurately. Willmarth and Roos [76] studied experimentally the effect of size of circular transducers. Value of $\sqrt{p^2}/\tau_w$ (ratio of root-mean-square wall pressure to the wall shear stress) is calculated for different radii of pressure transducers. The results are tabulated below [76, Fig. 6]

r/δ^*	$\sqrt{p^2}/\tau_w$
0.0	2.66
0.061	2.54
0.104	2.46
0.166	2.31
0.221	2.20

where δ^* is displacement thickness, $\sqrt{p^2}$ root mean square wall pressure and τ_w wall shear stress.

The root-mean-square wall pressure measured by a transducer of vanishingly small size is $\sqrt{p^2}/\tau_w = 2.66$ (obtained by extrapolation) and is approximately 13% higher than the value obtained by the transducer used by Willmarth and Wooldridge [72].

(b) Effect of vibration:

It was found that the signals caused by vibration of the pressure transducer amounted to less than 1/100 of the mean-square wall pressure fluctuations [72] and did not significantly contribute to the error in results.

(c) Effect of sound field:

While studying the effect of sound pressure, it was noted that spectral density of the sound had a peak at 135 cycles/sec [72] and at higher frequencies, spectral density was proportional to the inverse square of the frequency. The mean square sound pressure was 1/32 of the mean square wall pressure fluctuations. The signal from the pressure transducer may contain extraneous contributions due to the sound field in the working section in addition to contributions by other sources such as vibration and electronic noise. The sound pressure level was found to increase in the downstream direction [77]. At low free stream speed, the

mean square acoustic pressure amounted to 1.6% of the measured mean-square wall pressure at the upstream end of the working section and increased to 5.2% at the downstream end, while at higher flow speed, the corresponding values were 2.7 and 10.2%. It was also noted that the sound pressure signal had a broad band character, the power spectral density being highest at low frequencies and falling off with increasing frequency. In order to avoid these background effects, the spectral density measurements of the wall pressure were rejected for frequencies less than 300 cycles/sec. This frequency set the lower limit of frequency for measurements. The upper frequency limit for power spectral density measurements was set by the spectrometer used and for correlation work by the response of the tape-recorder.

It was experienced [77] that the pressure field can be divided into two families of wave-number components, one of high wave-number components and other of low wave-number components. The property of the high wave-number family at small separations that its components lose coherence more rapidly than the higher wave-number components, leads to the similarity of $\omega \xi_1/U_c(\omega)$ and $\omega \xi_3/U_c(\omega)$ (where ξ_1 and ξ_3 are the components of the separation vector in the streamline (x_1) and cross-stream (x_3) directions, U_c - convection velocity, ω - angular velocity). At the same time, the spectrum of correlated components is becoming progressively curtailed at high wave-numbers as separation

increases. At small separations, variations of longitudinal space-time correlations have sharp narrow peaks indicating a broad spectrum of correlated wave-numbers, but as separation increases, the peaks rapidly disappear and curves become broader and flatter, indicating a progressive loss of high wave-number contribution. The results of broad band convection velocity show that, initially, there is a strong contribution from the innermost part of the fully turbulent region of the constant stress layer and possibly the transition region also, but at larger separation distances the broad-band convection velocity rises rapidly towards the asymptotic value of 0.825 U_o characteristic of the large-scale structure of the field. This indicates that the contribution to the pressure correlation from the fine scale motion in this region close to the wall becomes small because of the rapid dissipation and dispersion of pressure sources by the high shear occuring there. The variation of broad band convection velocity suggests that the influence of the high wave-number family persists for the time taken for it to be convected a distance of at least $10\delta^*$.

III. DESIGN AND FABRICATION OF THE TEST MODEL

The test model consisted of the following two parts:

(a) Flat Plate Assembly

(b) Airfoil

The description of the flat plate assembly and the airfoil is as follows:

3.1 Flat Plate Assembly

The initial design concept of a flat plate turned out to be a design of complex flat plate assembly. The design required to satisfy many conditions such as obtaining a thick boundary layer, data transferring capability without any interference to the flow over the test model. Airfoil installation on both sides without bending, provisions for aligning it to the flow direction and injection of flow visualization agents. All the conditions were met by the design shown in Fig. 4. The design consisted of an assembly of two, (93.4 X 45.7 X 6.4) mm plates made of 2024 T4 bare aluminum alloy. Ribs, (6.4 X 12.7) mm were inserted between the two plates to keep the surfaces of the long plates free of curvature. The leading edge of the plate is made from 19 mm diameter aluminum bar. The trailing edge is formed by a 25.4 X 19 mm aluminum bar. The ribs and the plates are held

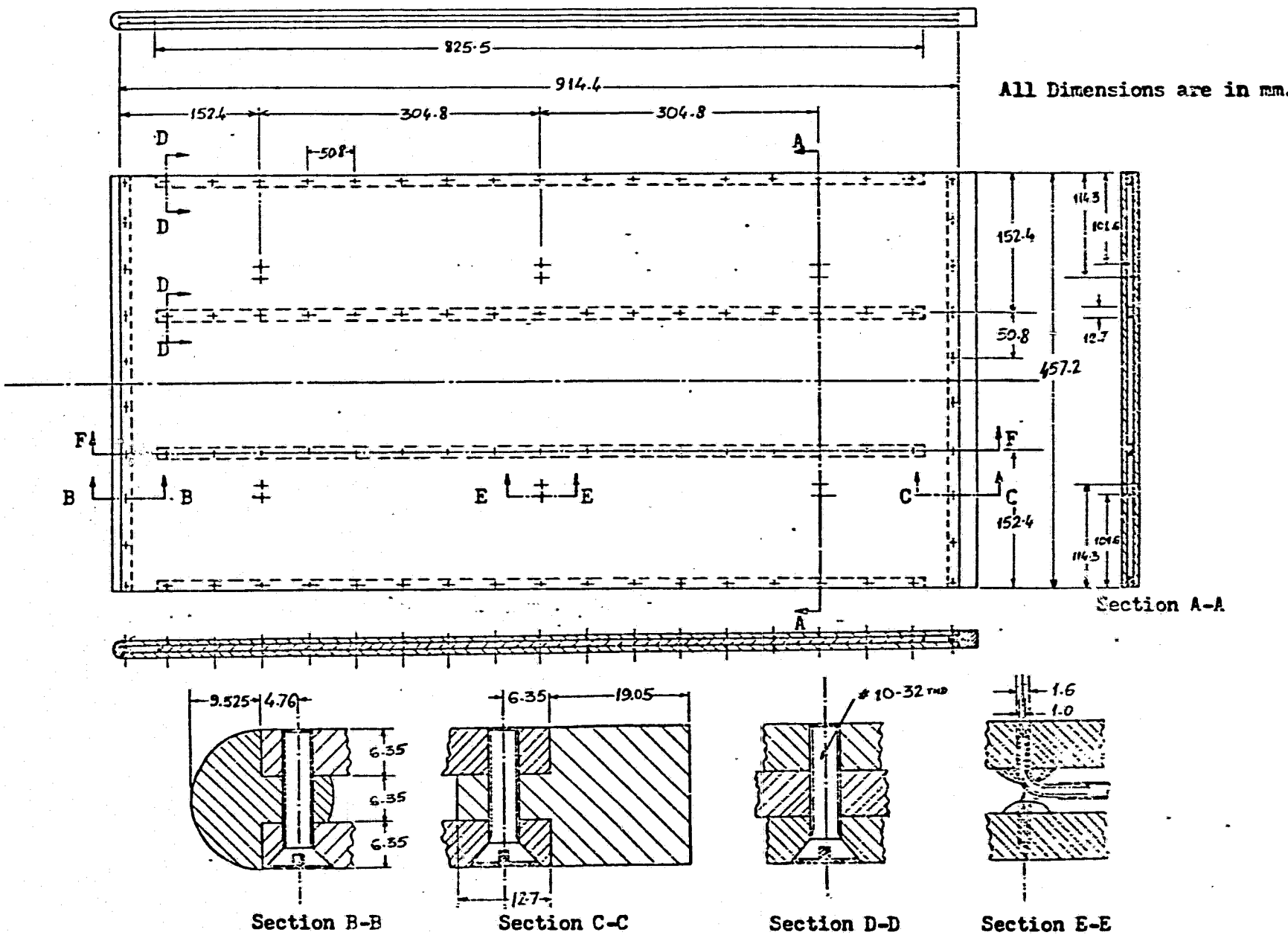

Figure 4. Flat Plate Assembly

together by equally spaced flush screws #10 - 32 thd. made from steel and spaced 50.8 mm apart. The static pressure holes are connected to polyethylene tubes through the stainless steel tubes. The fabrication of flat plate assembly was done with inhouse capability.

3.2 Airfoil

The base profile for the uncambered airfoil design was selected to be standard NACA 65 - 015. Based on the compromise of obtaining a thick boundary layer on the airfoil and its stall characteristics, the leading edge diameter was chosen to be 1.27 cm and the trailing edge diameter of 0.25 cm. The constant cross-section airfoil was split into two parts, each having a span of 21.9 $\pm$ 0.01 cm, to fit into the upper and lower sides of the flat plate assembly (Fig. 5). The decision to split the airfoil into two parts was made to reuse the flat-plate assembly for subsequent tests with cambered airfoils. A hole of diameter 0.95 cm was drilled through the airfoil's split parts to attach them to the two sides of the flat plate assembly with a bolt. The airfoil parts were manufactured by Kenric Industries, Conn. from aluminum. With the help of additional alignment points, the airfoil can be located on the flat plate assembly in any required position.

The test model assembly photograph is shown in Fig. 6.

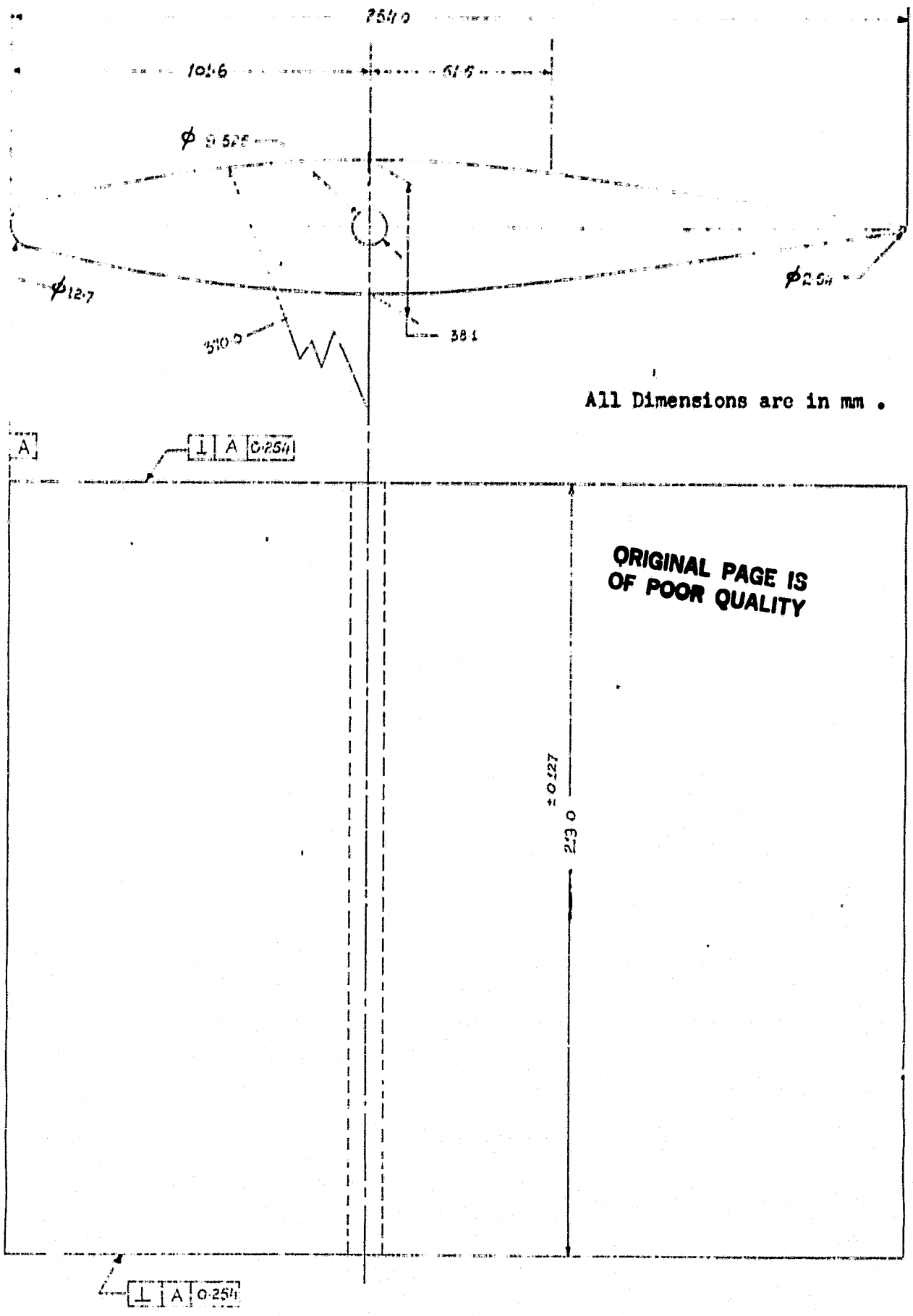

Figure 5. Airfoil for Corner Flow Turbulence Experiment.

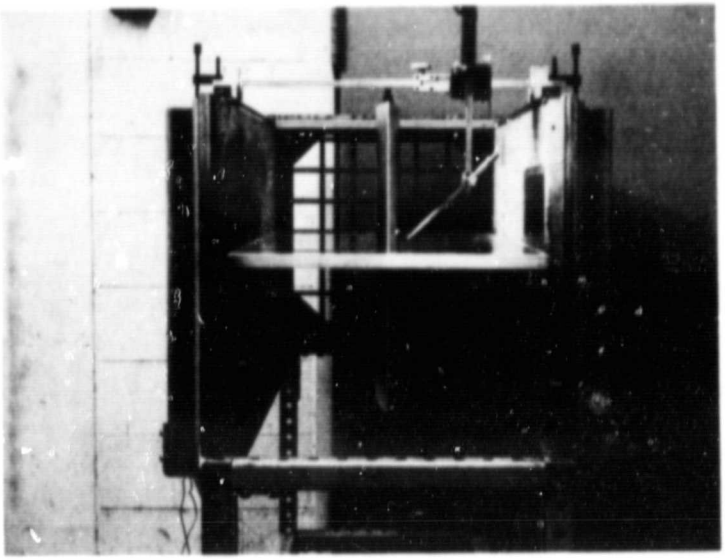

(a) Looking Upstream

(b) Looking Downstream

Figure 6. Photograph of the Test Model

IV. PRELIMINARY MEASUREMENTS

Preliminary measurements were required to select and set up the inlet flow conditions to establish the region of influence of the corner flow region, determine the overall magnitude of turbulence quantities, make an appropriate choice of probes and instrumentation for final measurements, and observe the overall structure of the corner flow region. To collect the above mentioned information, the preliminary measurements were carried out in the following three steps:

- o Boundary Layer Studies
- o Flow Visualization Studies
- o Turbulence Studies
  - (i) Turbulence Intensity
  - (ii) Turbulence Energy Spectra

All the foregoing measurements were conducted in the old Wind Tunnel while the new Wind Tunnel was being fabricated. The new Wind Tunnel will be used for final and extensive measurements after satisfactory completion of the shake down test.

4.1 Boundary Layer Studies

The main purpose of this study was to obtain a stable and thick turbulent boundary layer on a flat-plate ahead of the

beginning of the corner region. The location of the point of measurement is shown in Fig. 7, and is located 250 mm from the flat plate leading edge and 70 mm in the transverse direction from the blade leading edge. The standard boundary layer probe used was made by United Sensors, from 0.5 mm diameter stainless steel tube and flattened to 0.25 mm to give an elliptical cross section. The probe was connected to a pre-calibrated Validyne type transducer and the pressures were read on a DISA digital voltmeter.

The flat plate was set for zero incidence. The maximum difference of pressure between any two of the 12 static pressure holes was 0.2 mm of water. The boundary layer thickness was measured for the following four conditions in the test section:

(i) Flat plate without any aids to increase the boundary layer thickness.

(ii) Turbulence generating grid and flat plate (The grid was mounted 250 mm upstream the flat plate leading edge Fig. 8 and Fig. 9 show the grid configuration and its turbulence characteristics).

(iii) Flat plate and added roughness near the leading edge. (The roughness was created by the use of a 70 mm wide strip of a sand paper of 2 mm grit size and 15 grits/cm^2.)

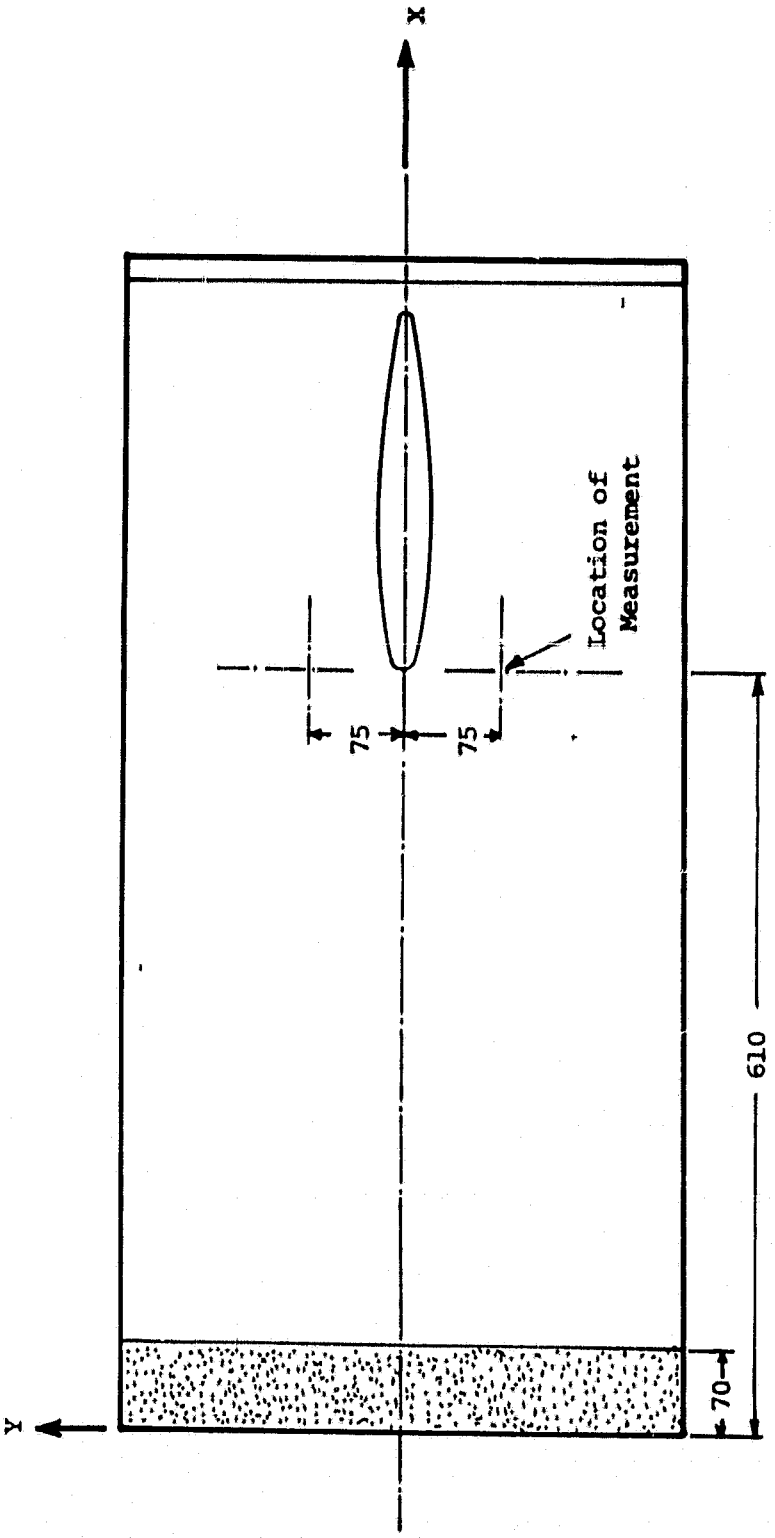

Figure 7. Location of Boundary Layer Measurement

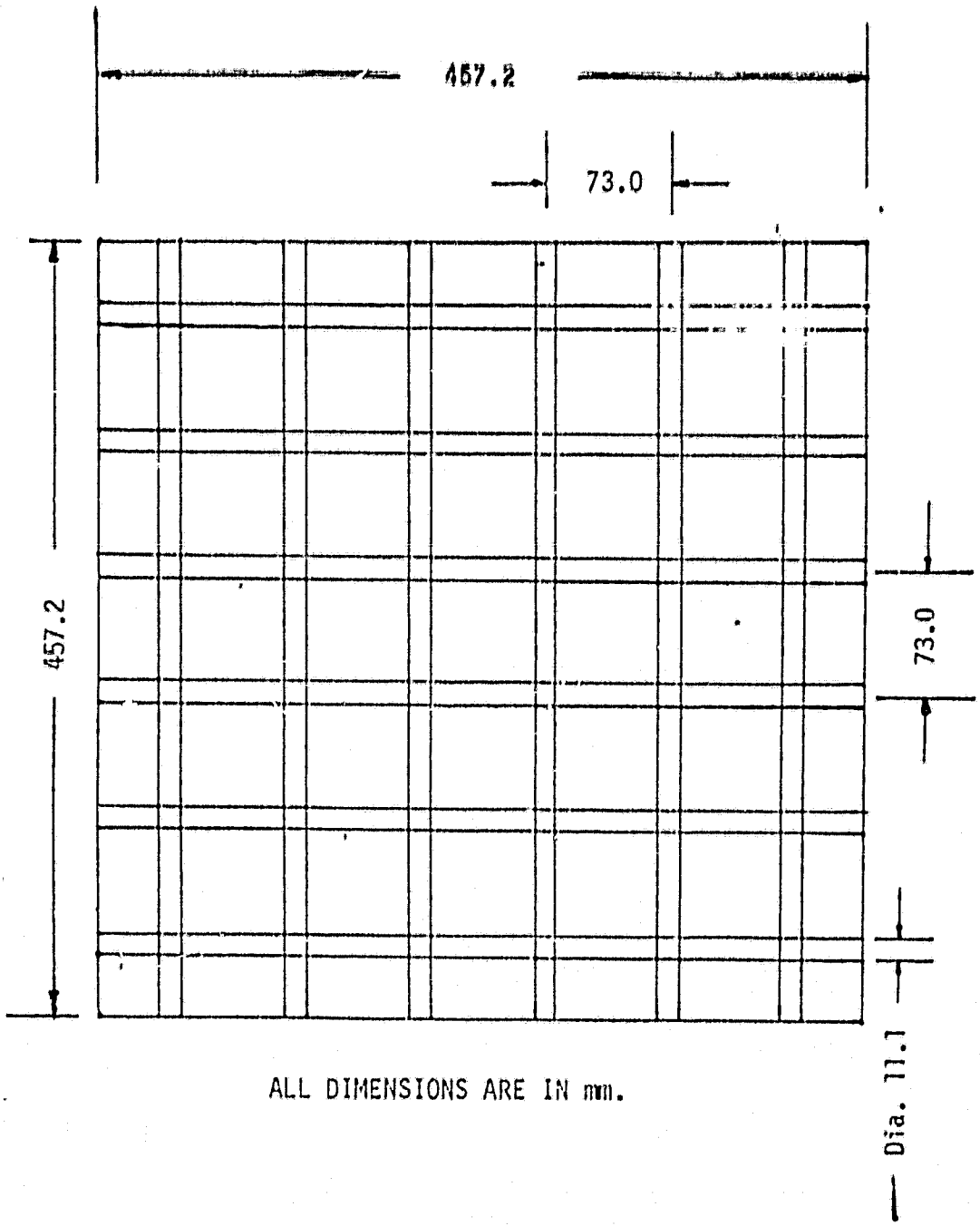

Figure 8. Configuration of the Grid

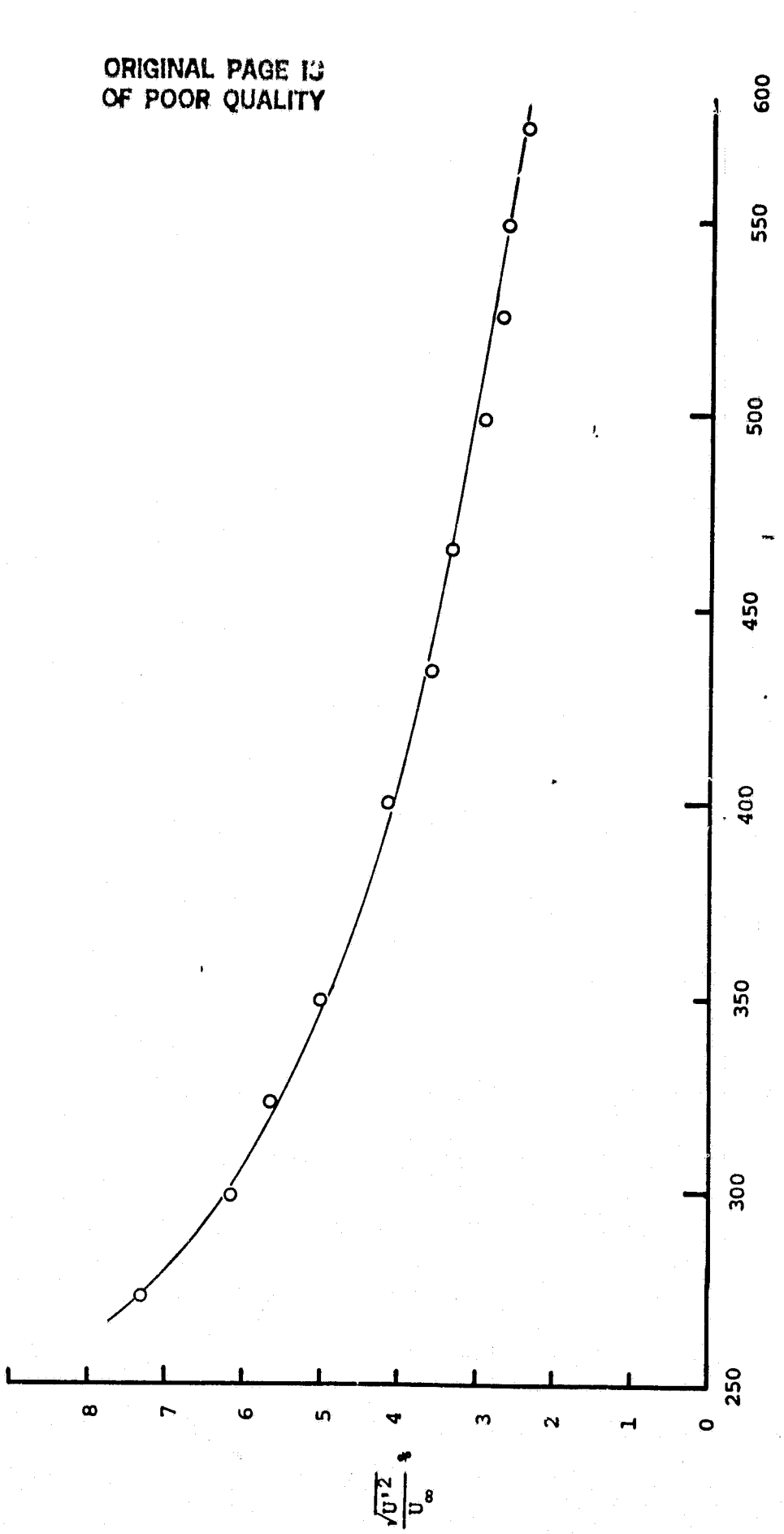

Figure 9. Variation of Longitudinal Component of Turbulence Intensity

(iv) Turbulence generating grid (same as described above in (ii) and flat plate with added roughness (same as described above in (iii). In this case the airfoil was also in place.

The experimental results on boundary layer thickness for the above mentioned four cases are summarized in Table (I) and the velocity profiles obtained are shown in Fig. 10 to 13.

The edge of the boundary layer was assumed to be the point where the edge velocity reaches 99.9 percent of the free stream value. It is clear from the results that a combination of turbulence generating grid and the flat plate with added roughness is the best choice to increase the boundary layer thickness.

4.2 Flow Visualization Studies

The main purpose of the flow visualization study was to obtain a qualitative picture of the structure of the corner flow. It was decided to carry out the investigation using two flow visualization techniques:

- o Surface oil flow visualization
- o Smoke filament flow visualization

It was expected that the first technique would provide a qualitative understanding of what was happening in the vicinity

TABLE (1)

Test Section Condition		Boundary Layer Thickness
(i)	Flat Plate	11 mm.
(ii)	Flat Plate with Inlet Free Stream Turbulence	15 mm.
(iii)	Flat Plate with 70 mm. Initial Length Roughened with Sand Paper	13.5 mm.
(iv)	Flat Plate with 70 mm. Initial Length Roughened with Sand Paper and Inlet Free Stream Turbulence	15.5 mm.

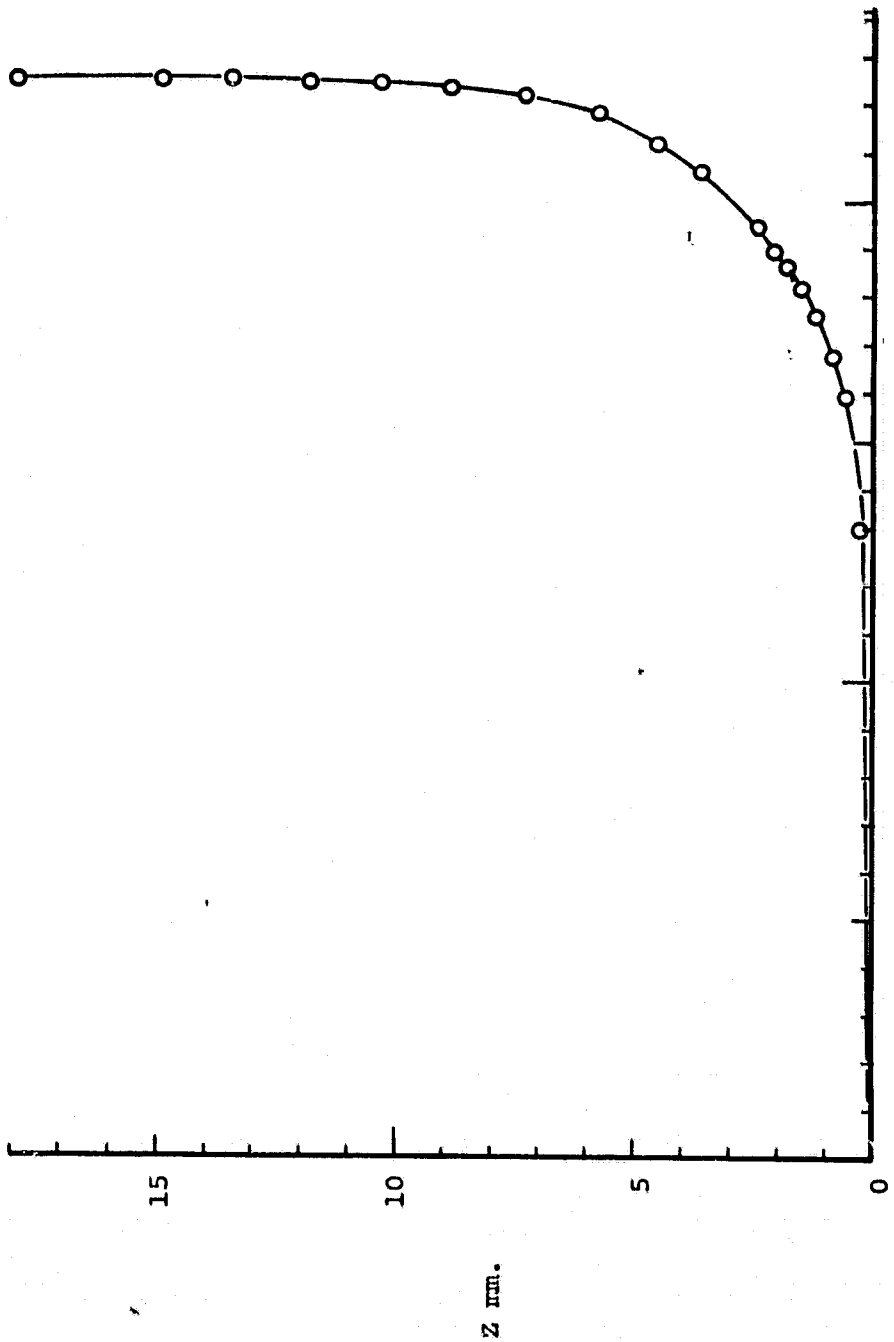

Figure 10. Mean Velocity Profile of the Boundary Layer on the Flat Plate

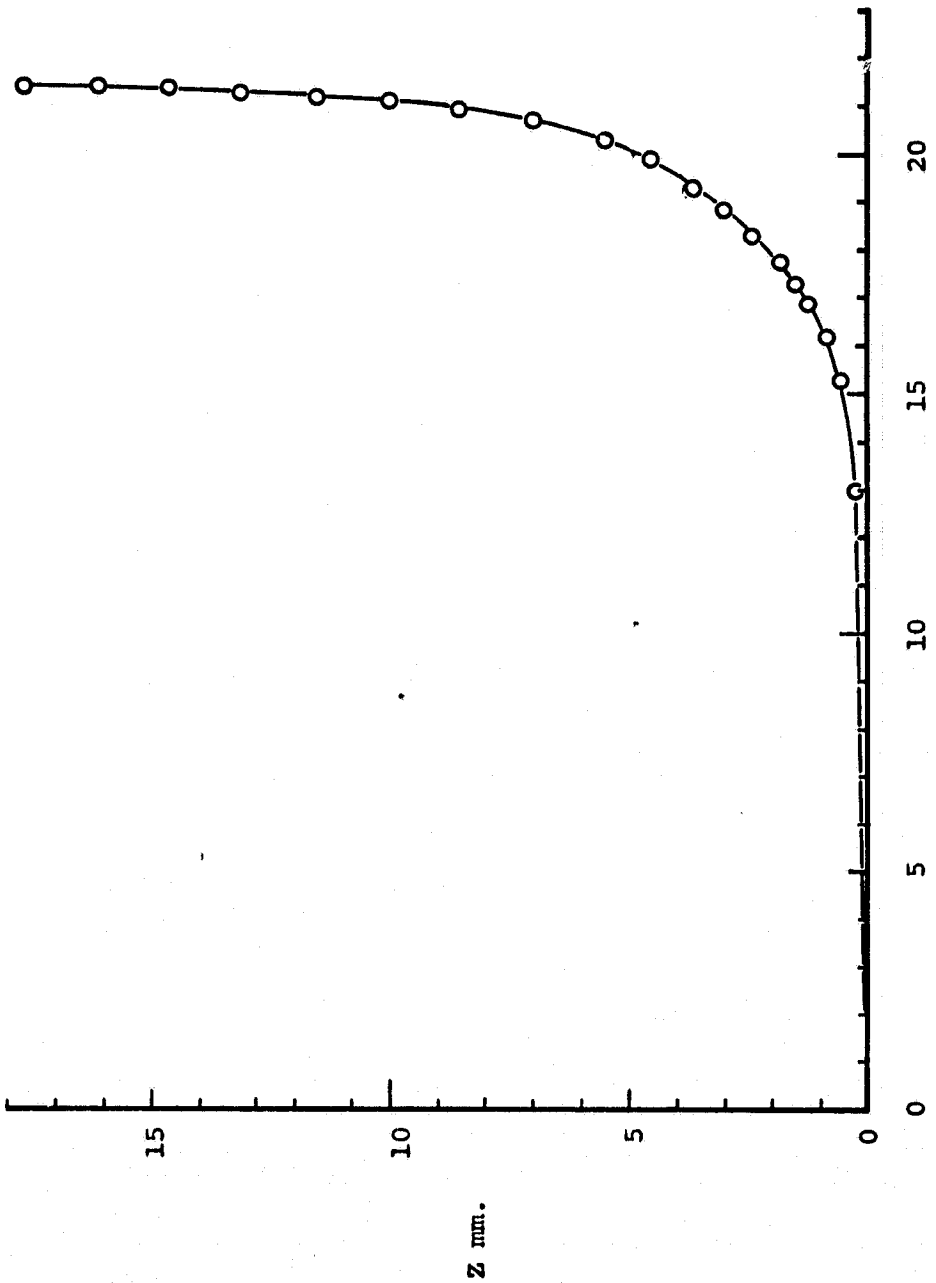

Figure 11. Mean Velocity Profile of the Boundary Layer on the Flat Plate with Inlet Free Stream Turbulence

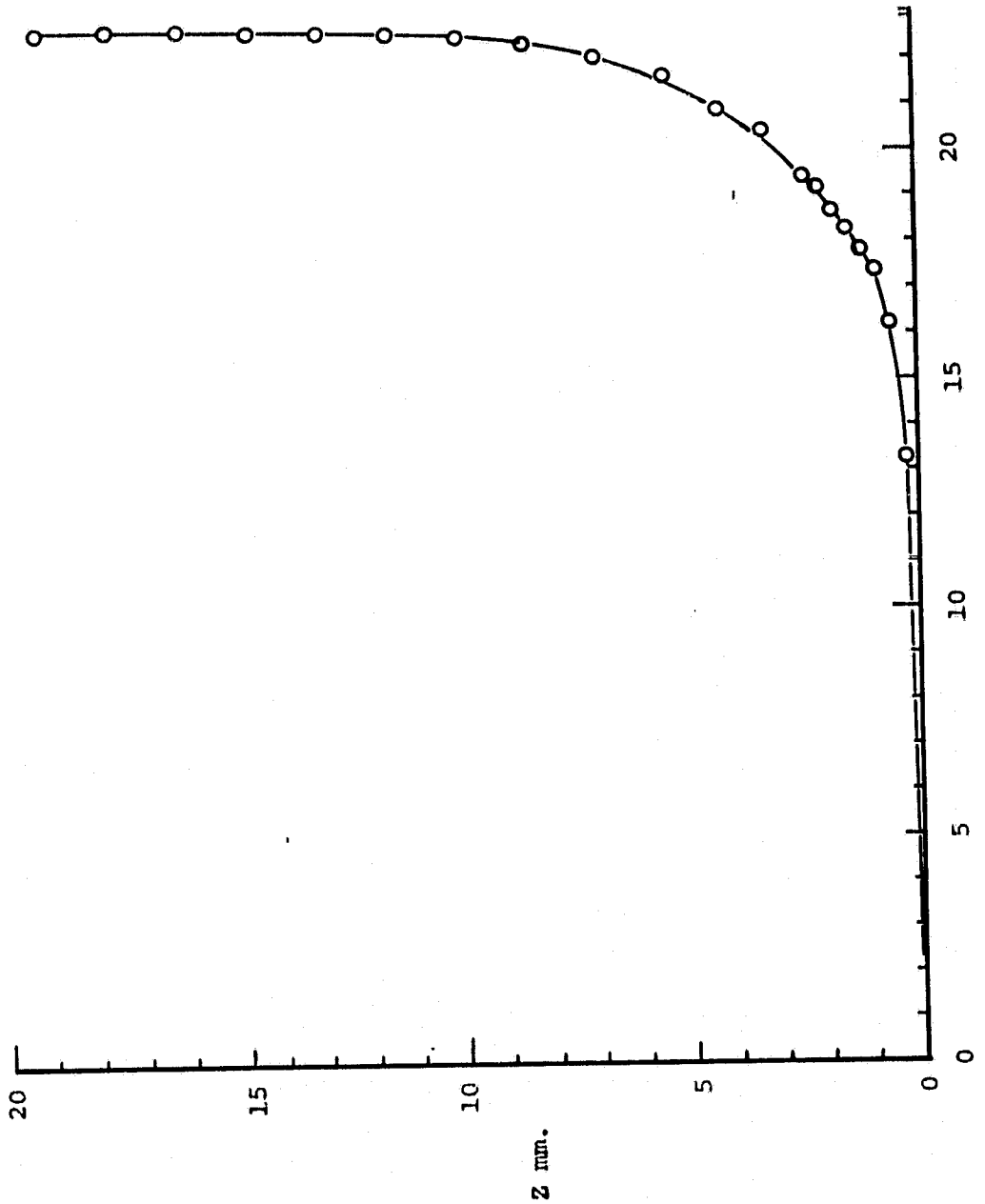

Figure 12. Mean Velocity Profile of the Boundary Layer on the Flat Plate with 70 mm. Initial Length Roughened with Sand Paper

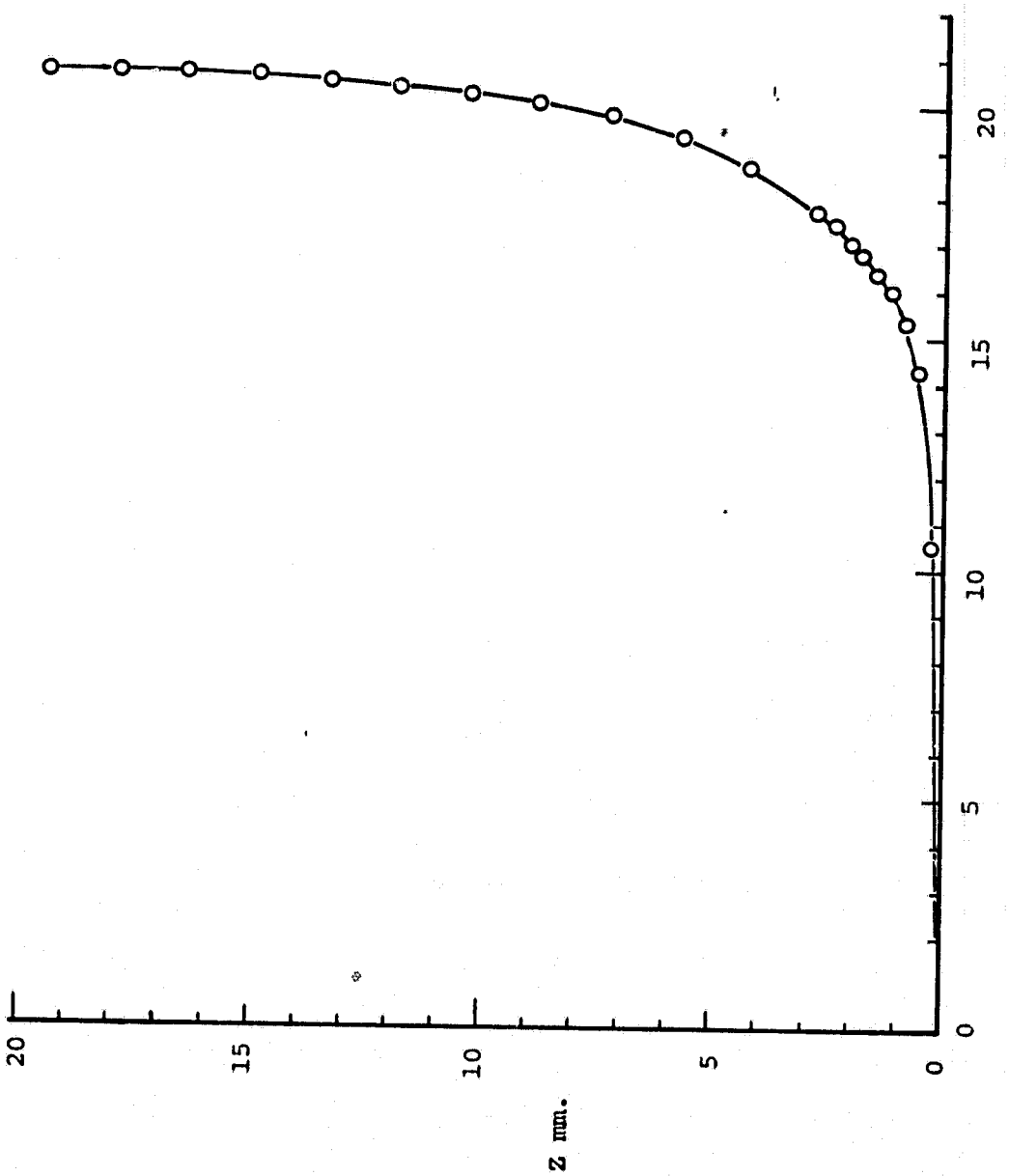

Figure 13. Mean Velocity Profile of the Boundary Layer on the Flat Plate with 70 mm. Initial Length Roughened with Sand Paper and Inlet Free Stream Turbulence

of the surface. The second technique combined with high speed motion picture and motion analyzer would provide a clear picture of what is happening in the corner region away from the surface.

The flow visualization experiments using the first technique were quite successful. However, in the second technique, difficulties arose in creating thick smoke and sustaining it up to the distances of interest. Nevertheless, some static photographs were obtained which did not provide much information. Effort to perfect this technique for highly diffusive flows is still continuing in order to obtain the spacial information concerning the fluid flow phenomenon in the corner region.

The oil used in the surface flow visualization experiment was #2 Diesel. Lampblack and titanium dioxide were used as pigments and oleic acid as dispersing agent depending upon the information required. Lampblack with very small amount of oleic acid(and sometimes without this dispersing agent) mixed with #2 Diesel to form a moderately thin paint gave good results when an over-all flow pattern was required. However, for a finer flow pattern inside the overall flow pattern, lampblack or TiO_2 mixed with oleic acid in the ratio 4:1, dissolved in #2 Diesel to form a moderately thin paint were found to be more suitable. A very thin paint made from lampblack and #2 Diesel, with or without oleic acid was suitable, when it was required

to get an understanding of the strength of vortices on the surface and when information was needed concerning the time taken for a definite flow pattern to develop.

In the smoke filament flow visualization experiments, titanium tetrachloride and the moisture present in the air react and generate a dense smoke, containing HCℓ and suspended TiO_2. When the smoke passes through the tubes, TiO_2 deposits inside the tube passage and blocks its passage. The blockage hindered the process of continuous injection of thick smoke into the flow passage. It was not found possible to use tubes less than 3 mm in diameter at all. Therefore, the technique used was to dip the tube in $TIC\ell_4$ and fix it in the position required. One motion picture was taken with this method. Another motion picture was taken by inserting some of the liquid $TIC\ell_4$ upstream of the airfoil. It was not possible to obtain any information from these two films, nor from static photographs also taken. In this report, although not presented, the photographs are kept in file.

4.2.1 Experimental Results on Surface Oil Flow Visualization Studies

The photographs Fig. 14 to 19 on surface oil flow visualization studies reveal the nature of the flow stream lines near the leading edge, mid chord position and trailing

edge of the corner region. The photographs also qualitatively indicate the dimensions of the region of influence of corner flow for the test model used. Although we have not yet made a detailed analysis of all the photographs, nevertheless, the following observations may be of interest:

From the patterns of streamlines on the flat plate near the airfoil, it was observed that the nodal point of separation occurs about 12 mm upstream of the leading edge of the airfoil (Fig. 14) and the curved separation line, gradually displaces away from the airfoil to about 20 mm at an axial distance of 50 mm from the leading edge. The separation line then gradually draws closer to the airfoil. At an axial distance of 130 mm from the leading edge, it is at a distance of 14 mm from the blade surface. The separating line then becomes almost parallel to the surface between axial distances of 130 to 165 mm from the leading edge, before again displacing away from the airfoil surface (Fig. 15). Near the trailing edge the separating line is 19 mm away from the wake center-line (Fig. 16). A small corner stall appears to be present from about 10 mm upstream of the trailing edge (Fig.17). The region of "horse shoe" vortex is between the separating stream line and the airfoil surface.

With the span of the airfoil horizontal, the pattern near the flat plate on the leading edge of the airfoil, the streaks in the region 1.5 mm to about 8 mm span bend towards

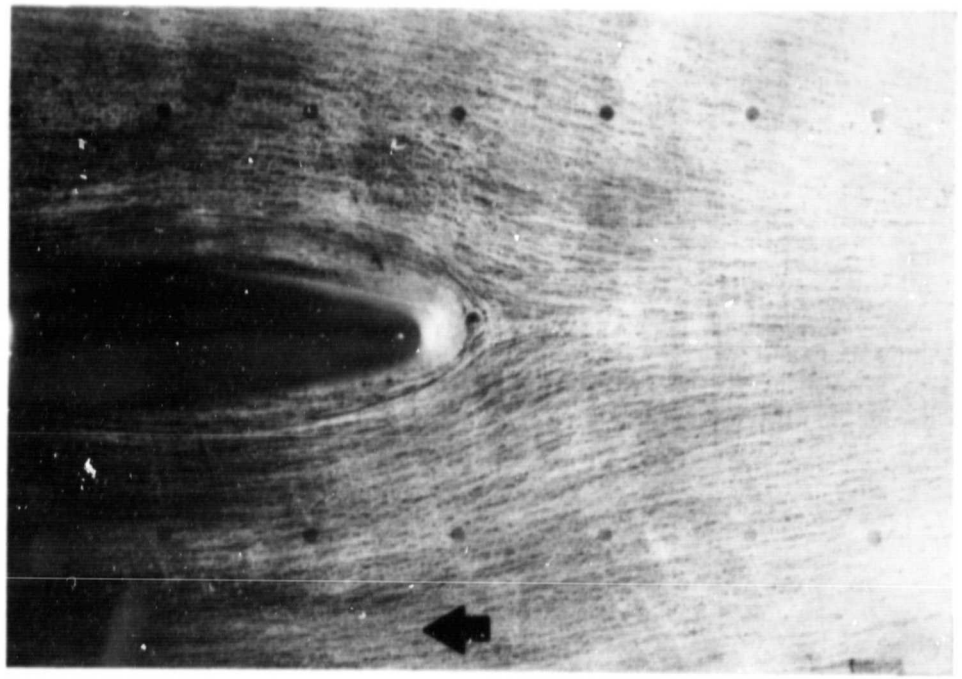

Figure 14 - Photograph of Streamline Pattern Obtained From Surface Oil Flow Visualization Experiment. Arrow shows the Direction of Flow.

(i) Location of Observation: Leading Edge Region of Airfoil on the Flat Plate

(ii) Camera Position: Top of Test Section

(iii) Special Feature: Medium Thick Solution of #2 Diesel oil, Lampblack and Oleic Acid.

ORIGINAL PAGE
BLACK AND WHITE PHOTOGRAPH

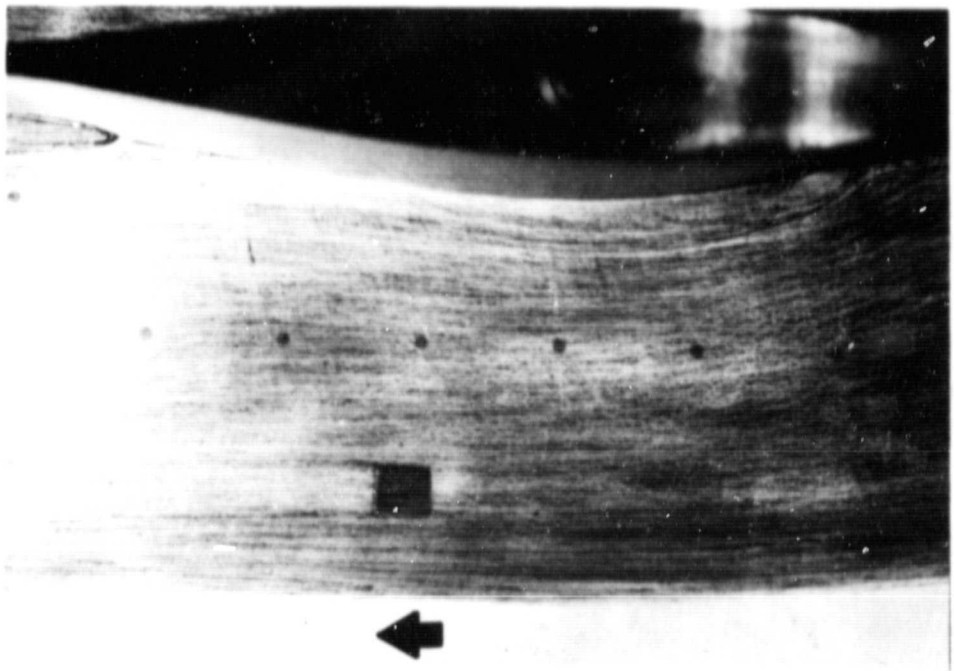

Figure 15 - Photograph of Streamline Pattern Obtained From Surface Oil Flow Visualization Experiment. Arrow Shows the Direction of Flow.

(i) Location of Observation: Mid Chord Region of Airfoil on Flat Plate

(ii) Camera Position: Top of Test Section

(iii) Special Feature: Medium Thick Solution of #2 Diesel Oil, Lampblack and Oleic Acid.

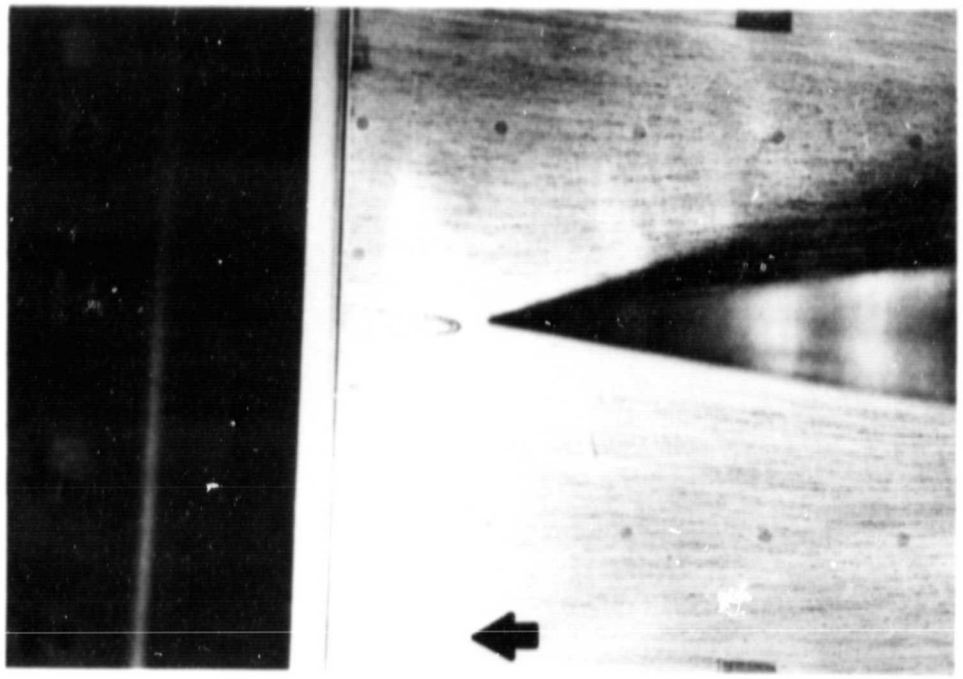

Figure 16 - Photograph of Streamline Pattern Obtained From Surface Oil Flow Visualization Experiment. Arrow Shows the Direction of Flow.

(i) Location of Observation: Trailing Edge Region of Airfoil on Flat Plate

(ii) Camera Position: Top of Test Section

(iii) Special Feature: Medium Thick Solution of #2 Diesel Oil, Lampblack and Oleic Acid.

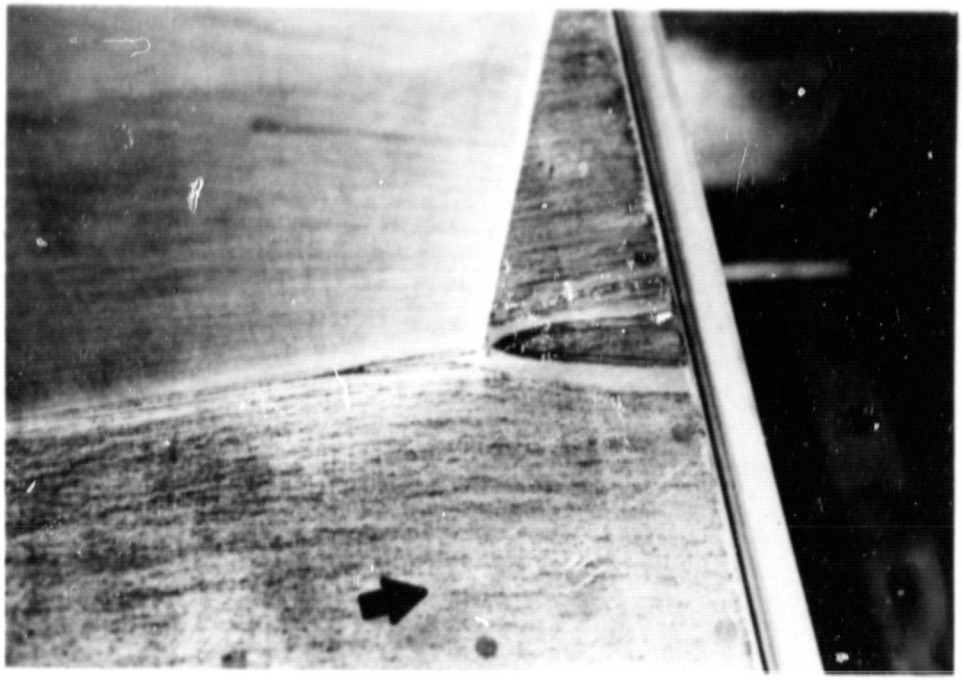

Figure 17 - Photograph of Streamline Pattern Obtained From Surface Oil Flow Visualization Experiment. Arrow Shows the Direction of Flow.

(i) Location of Observation: Trailing Edge Region of Corner, Flat Plate and Upper Airfoil.

(ii) Camera Position: Top of Test Section on Right at 45^{o} Downstream the Test Model.

(iii) Special Feature: Medium Thick Solution of #2 Diesel Oil, Lampblack and Oleic Acid.

the flat plate. Slightly downstream, close to the flat plate (1.5 mm - 3 mm), small streaks away from the flat plate appear and a similar pattern keeps enlarging to about 3 mm, near the trailing edge. At about 100 mm from the leading edge, the general trend of all the streamlines are away from the surface of the flat plate. These results are from measurements on the airfoil after completion of the test. We could not,however, obtain good photographs.

Outside these regions described, the general trend of the streamlines show the displacement effect of the boundary layer on the perpendicular surface.

From these patterns, it is evident that a "horse shoe" vortex has formed at the leading edge of the airfoil from the vortex tube in the boundary layer of the flat plate. The diffusive effect of Reynolds stress reduces the strength of the vortex downstream. The Secondary Flow of the First Kind seems to be dominant in most of the region.

Very near the corner, from about mid chord, there seems to be some Secondary Flow of the Second Kind present. The growth of the Double Vortex due to this is evident from (Fig. 18,19). However, away from this narrow strip, Secondary Flow of the First Kind is dominant all the way up to the trailing edge. The appearance of Secondary Flow of the Second Kind is also confirmed through turbulence spectra reported in Section (4.3).

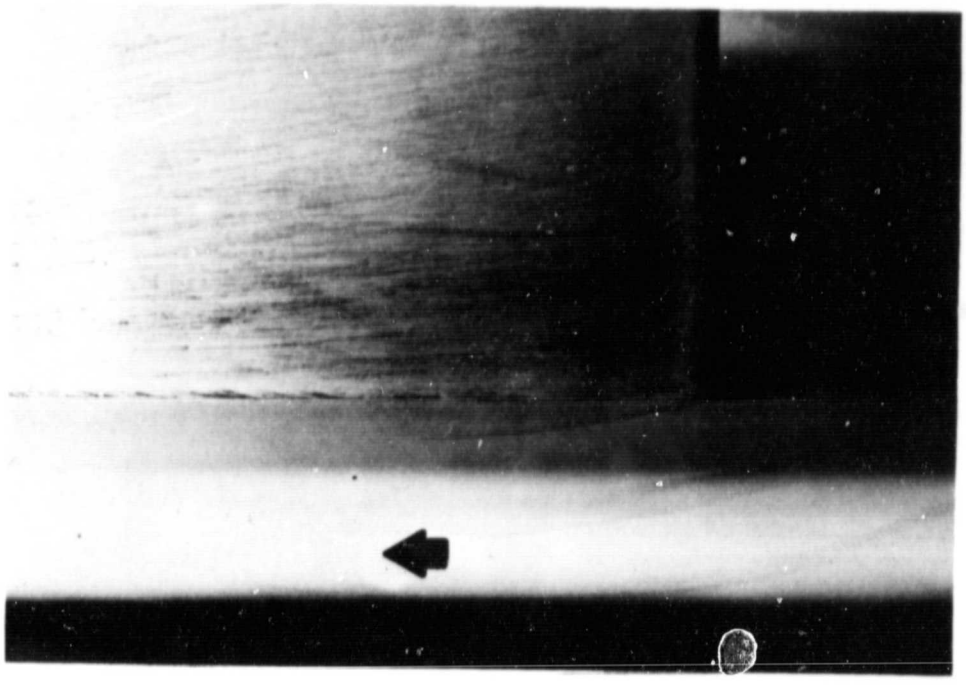

Figure 18 - Photograph of Streamline Pattern Obtained From Surface Oil Flow Visualization Experiment. Arrow Shows the Direction of Flow

(i) Location of Observation: Leading Edge Region on Upper Airfoil

(ii) Camera Position: Parallel to Flat Plate

(iii) Special Feature : Medium Thick Solution of #2 Diesel oil, Lampblack and Oleic Acid

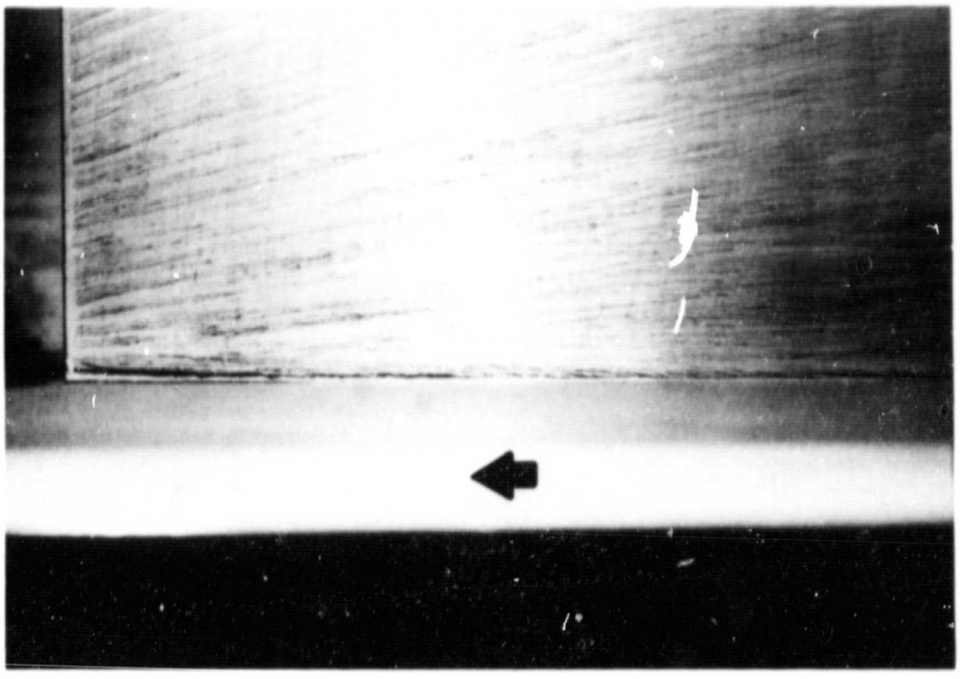

Figure 19 - Photograph of Streamline Pattern Obtained From Surface Oil Flow Visualization Experiment. Arrow shows the Direction of Flow

(i) Location of Observation: Trailing Edge Region on Upper Airfoil

(ii) Camera Position: Parallel to Flat Plate

(iii) Special Feature: Medium Thick Solution of #2 Diesel Oil, Lampblack and Oleic Acid.

4.3 Turbulence Studies

Turbulence measurements were conducted to evaluate the overall turbulence properties of the corner region. The properties measured were longitudinal component of turbulence intensity and turbulence energy spectra. The hot-wire probe was used in these measurements. The sensor of the probe was 4 micron diameter and 1 mm long. The hot-wire probe sensor material was tungsten. The anemometer, R.M.S. and digital voltmeter used in the experimentation were DISA made. The energy spectra were measured with the help of an ultrasonic spectrum analyzer.

The location of measurements for both the longitudinal component of turbulence intensity and the turbulence energy spectra are shown in Fig. 20. There were five axial stations of measurements and four points of measurements (a,b,c,d) at each axial station. The results obtained on longitudinal component of turbulence intensity are summarized in Table(2). The values of turbulence intensity are presented non-dimensionalized with respect to local mean velocity and free stream mean volocity.

The maximum variation of turbulence intensity along the chord length is observed for point 'b'. The trend in variation of turbulence intensity for points a,b,c and d are not consistent and apparently are correlated to the development

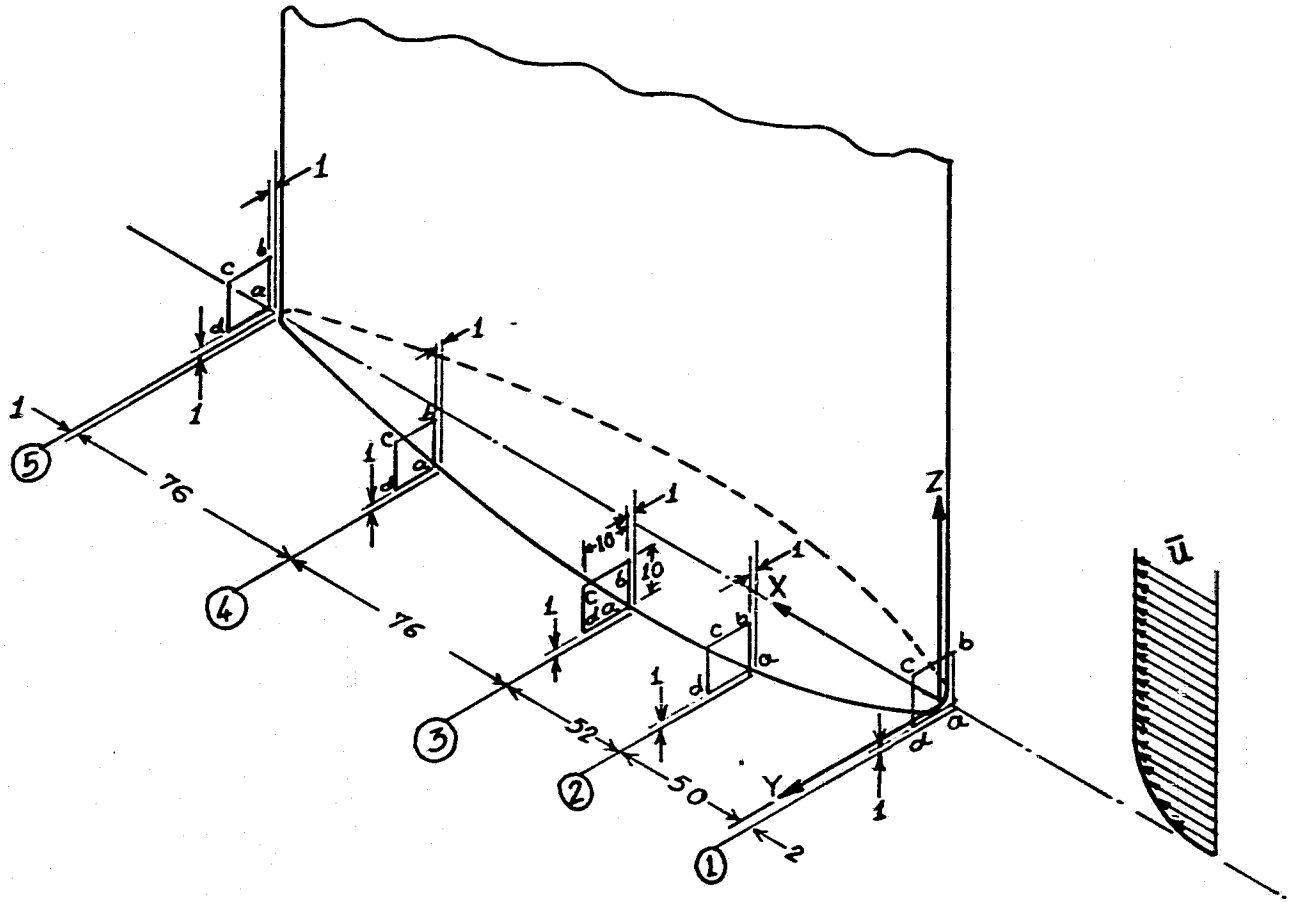

All Dimensions are in mm.

Figure 20. Schematic of Stations and Locations of Measurements for Turbulence Spectra and Intensity

TABLE (2)

TURBULENCE INTENSITY

Station Located		1	2	3	4	5
a	(i)	28.96	6.27	6.48	9.35	16.89
	(ii)	5.47	6.08	6.23	5.91	5.73
b	(i)	17.15	6.01	7.42	10.46	24.72
	(ii)	4.89	6.09	7.30	7.44	7.36
c	(i)	8.23	5.48	5.10	5.60	8.70
	(ii)	6.31	5.47	5.23	5.27	7.03
d	(i)	12.79	6.87	8.58	11.06	12.64
	(ii)	8.09	6.00	7.49	8.39	7.73

(i) With respect to Local Mean Velocity
(ii) With respect to Free Stream Mean Velocity 23.4 m/sec.

of corner flow. A detailed and closer examination of this phenomenon will be made after we have completed the detail measurements in this region.

The spectra were taken for a sweep width of 30,000HZ. The spectra are presented in photographs (Fig. 21-40). The ordinate represents a Db scale while the abscissa represents frequency. The photographs on spectra show that there is an increase in percentage of total kinetic energy contained in the smaller eddies at station 2 for points a and b.

Along point 'a' which is the point of measurement closest to corner, the increase in the energy at high frequency at station 2 may be attributed to the formation of double vortex. It appears that the scale of double vortex formation is of the order of 2 mm, which is nearly the same as the distance of point 'a' from the corner. However, there is not much change in spectrum from station (2) to (3).

From the oil film flow visualization, it is observed that double vortex formation almost coincides with the increase in the energy contained in larger vortices. However, reduction in turbulence intensity can not be explained at this time.

Along point 'b' which is in the outer region of the incident boundary layer, the spectrum at section 2 shows marked increase in energy of small eddies and turbulence intensity.

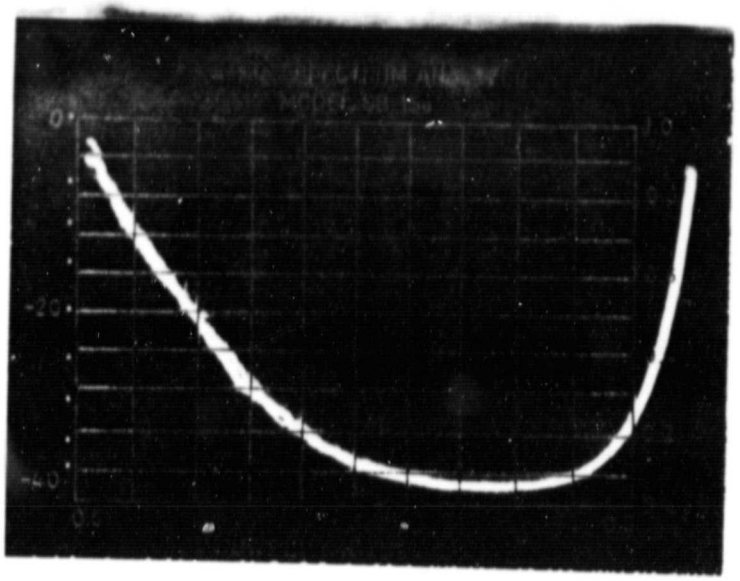

Figure 21. (Location 1a)

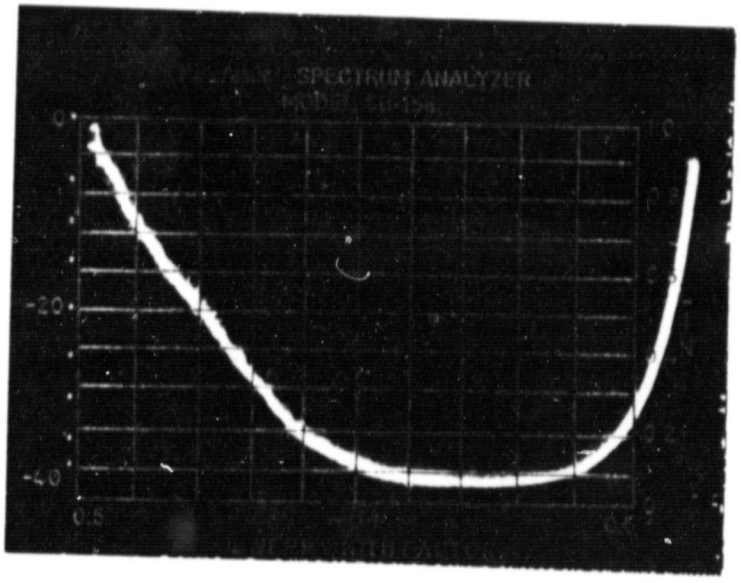

Figure 22. (Location 1b)

ORIGINAL PAGE
BLACK AND WHITE PHOTOGRAPH

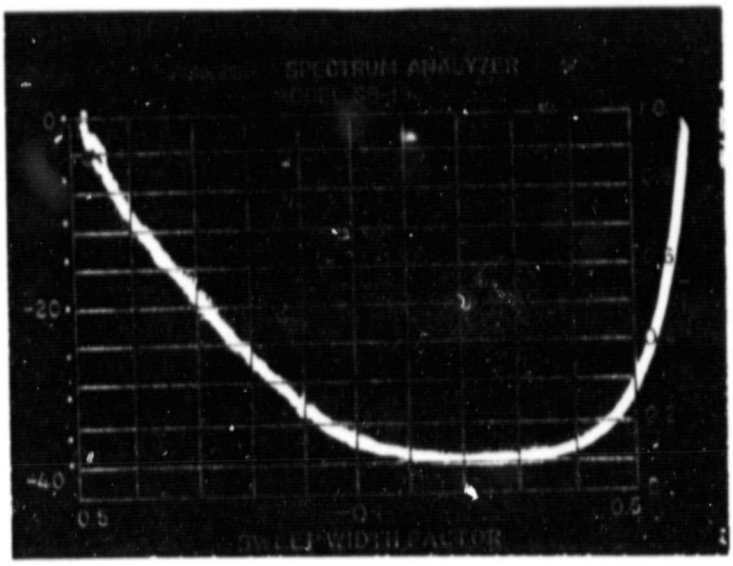

Figure 23. (Location 1c)

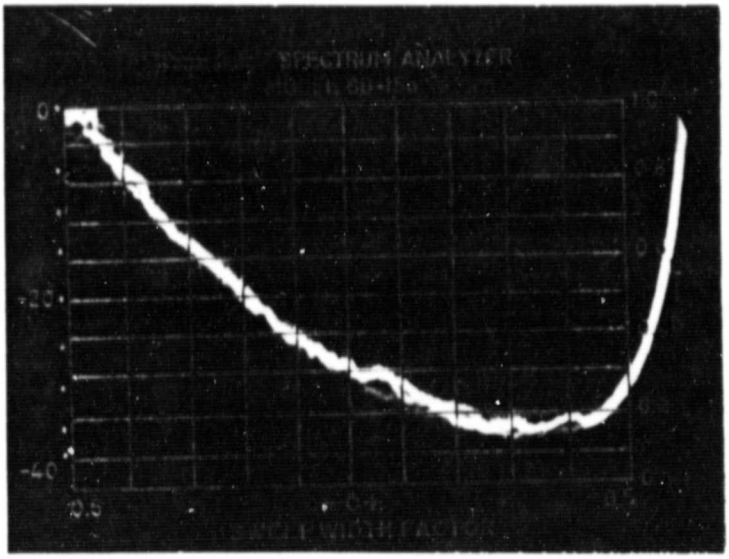

Figure 24. (Location 1d)

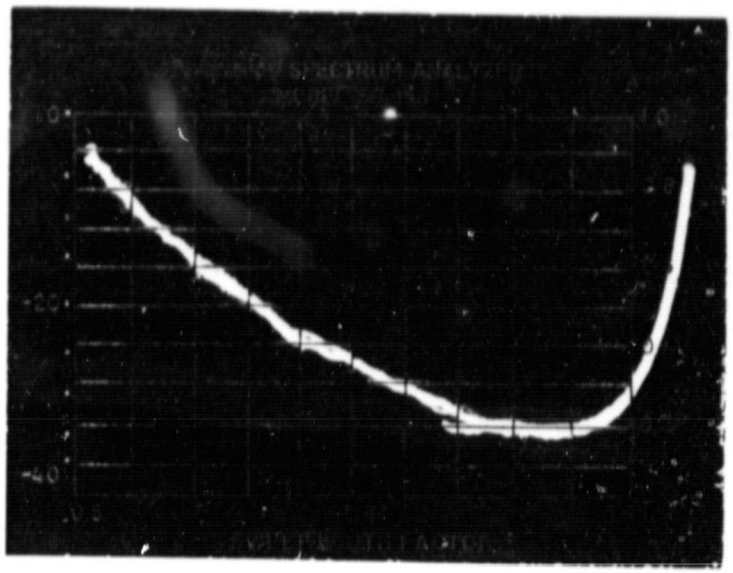

Figure 25. (Location 2a)

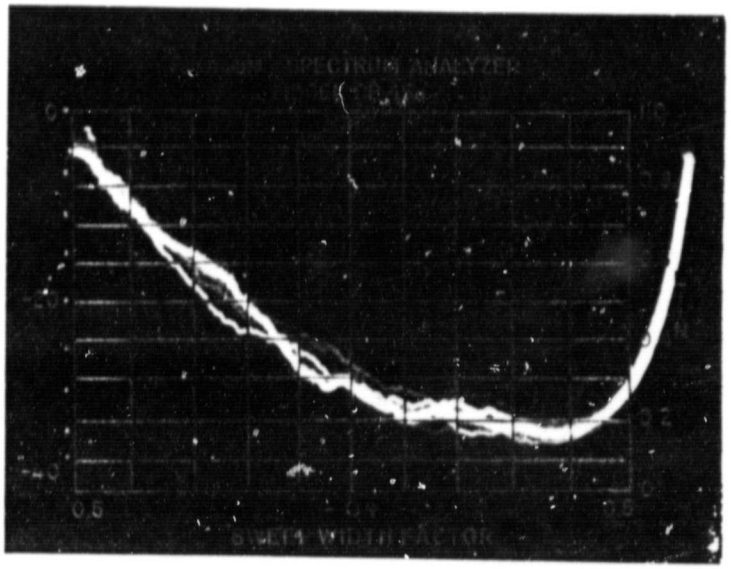

Figure 26 (Location 2b)

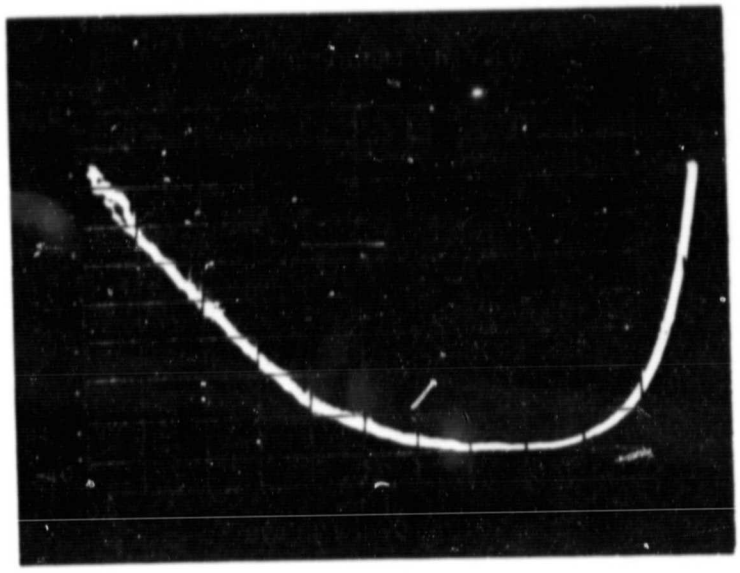

Figure 27. (Location 2c)

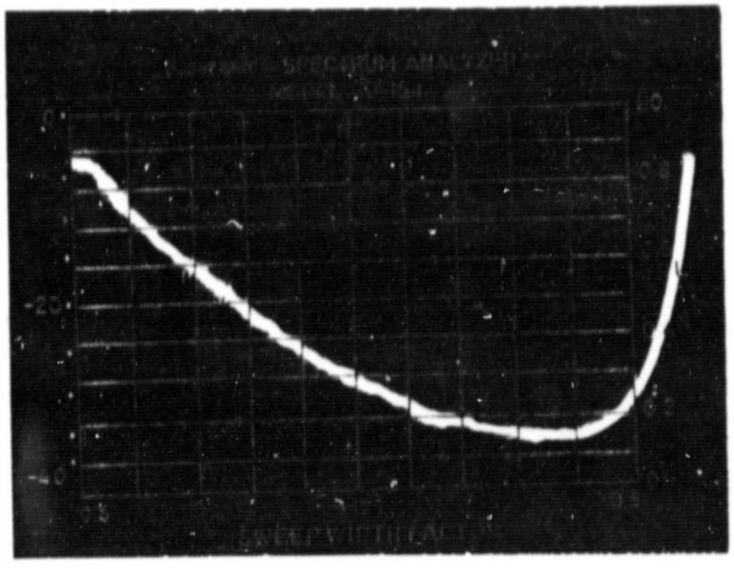

Figure 28. (Location 2d)

ORIGINAL PAGE
BLACK AND WHITE PHOTOGRAPH

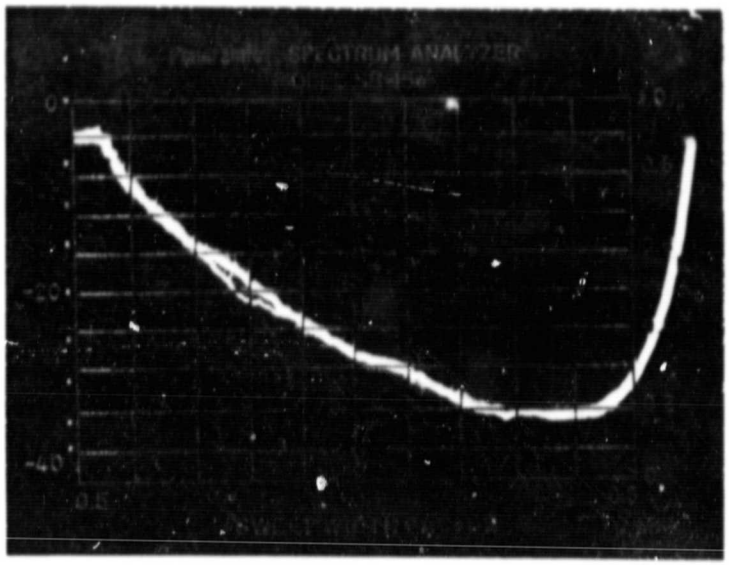

Figure 29. (Location 3a)

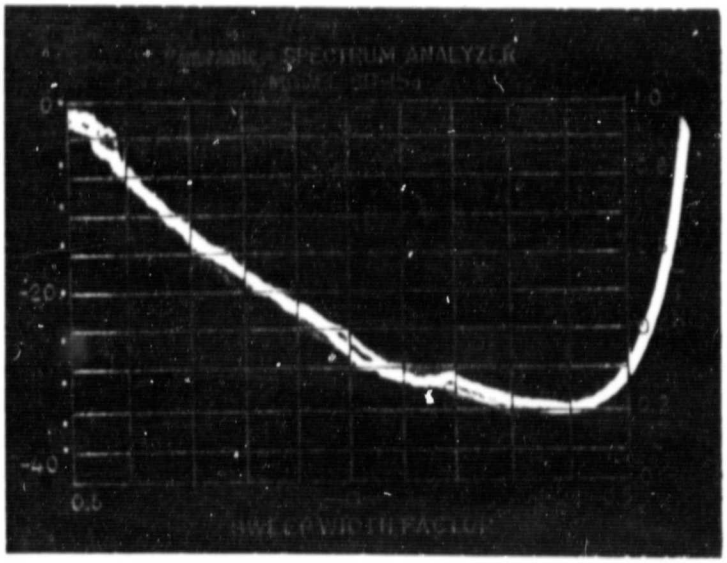

Figure 30. (Location 3b)

ORIGINAL PAGE
BLACK AND WHITE PHOTOGRAPH

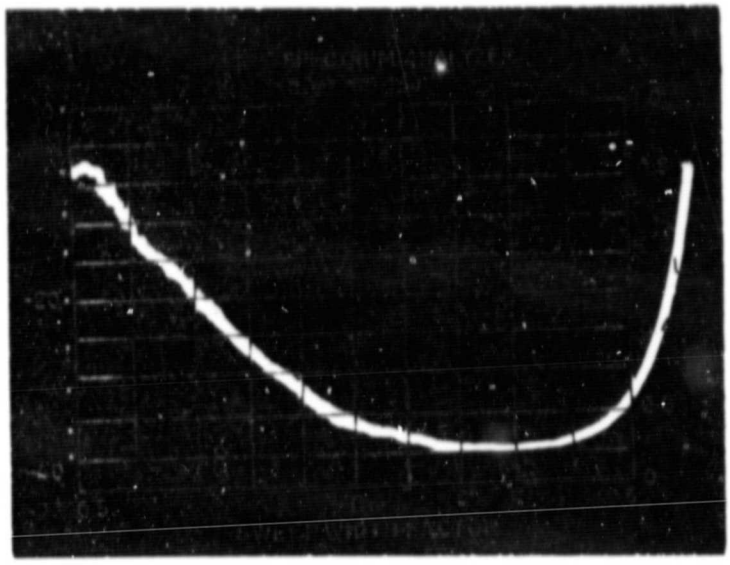

Figure 31. (Location 3c)

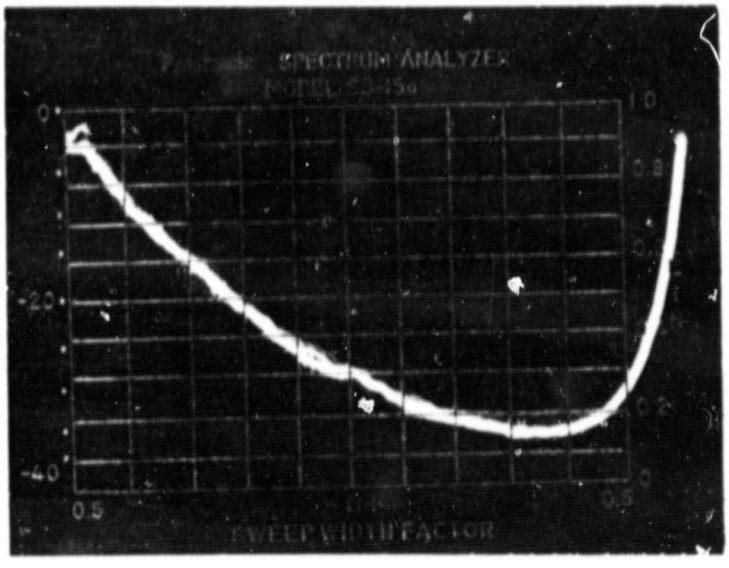

Figure 32. (Location 3d)

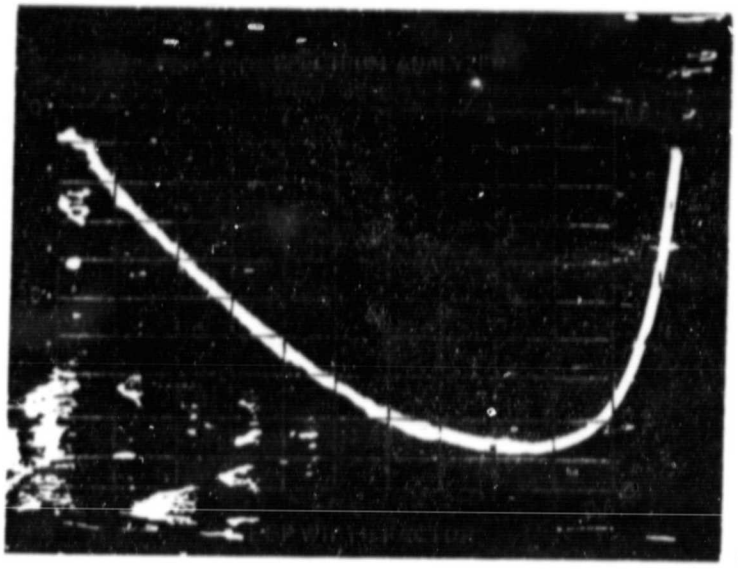

Figure 33. (Location 4a)

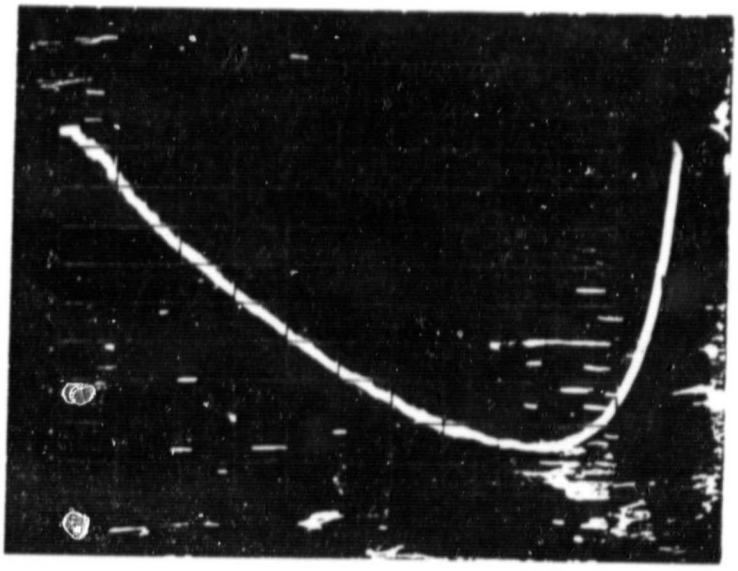

Figure 34. (Location 4b)

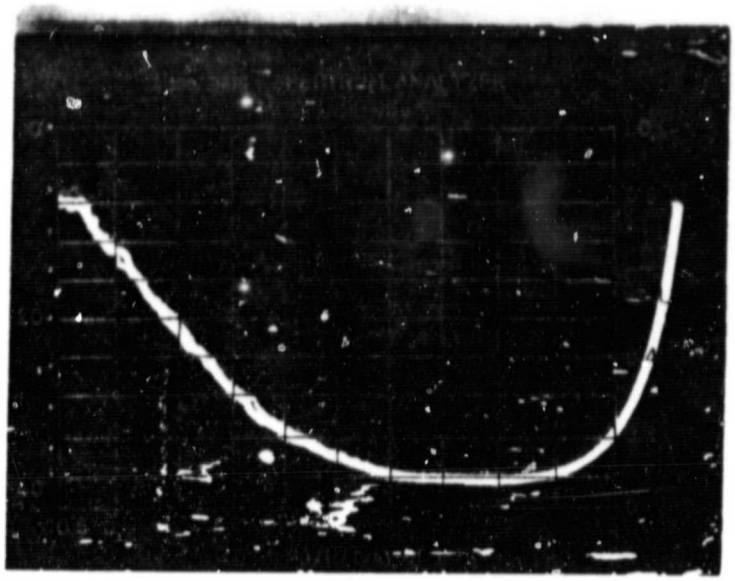

Figure 35. (Location 4c)

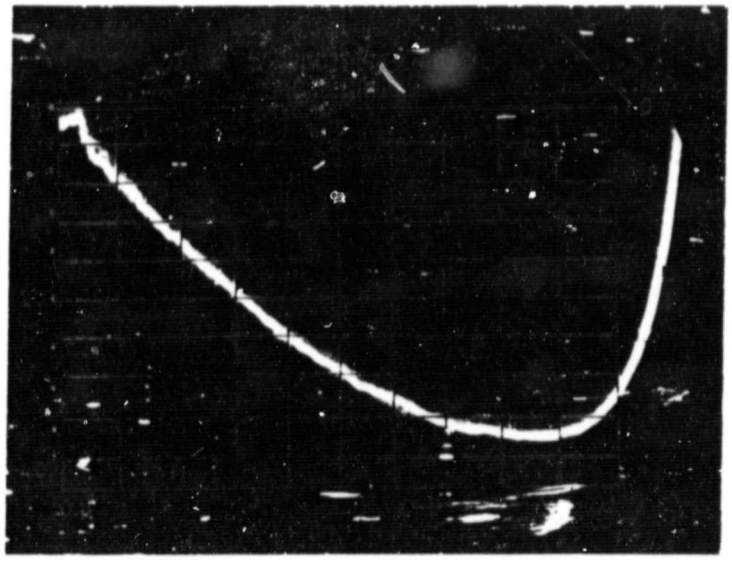

Figure 36. (Location 4d)

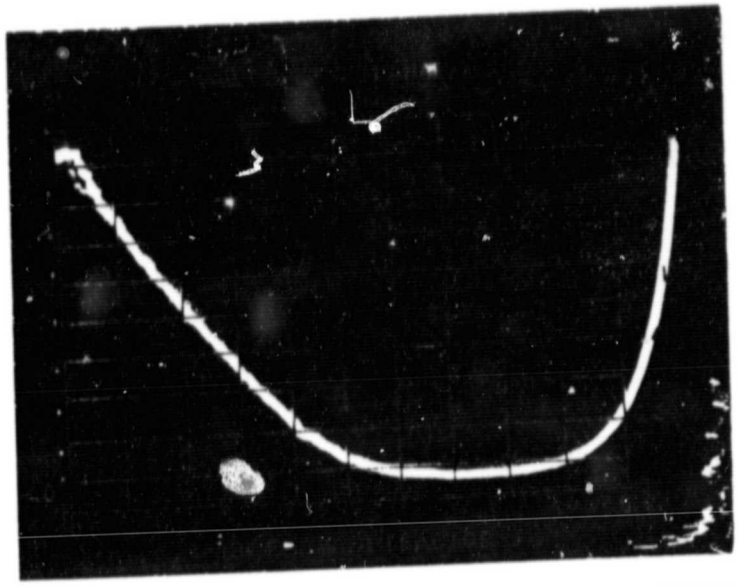

Figure 37. (Location 5a)

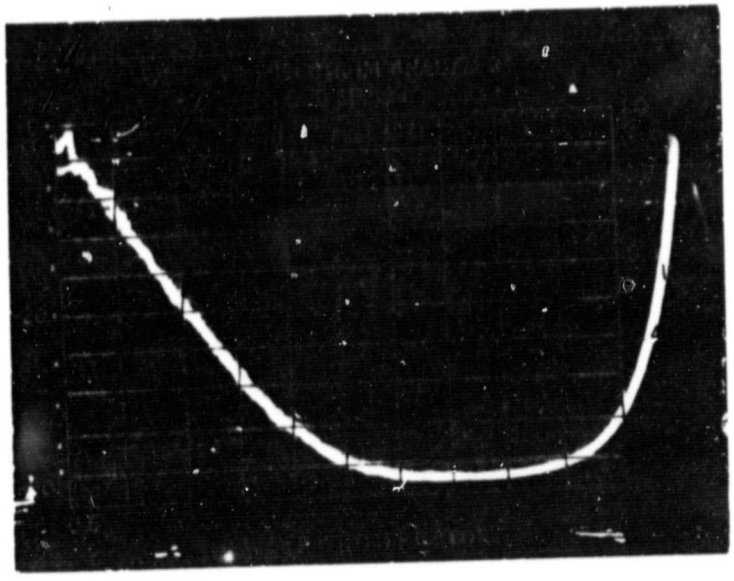

Figure 38. (Location 5b)

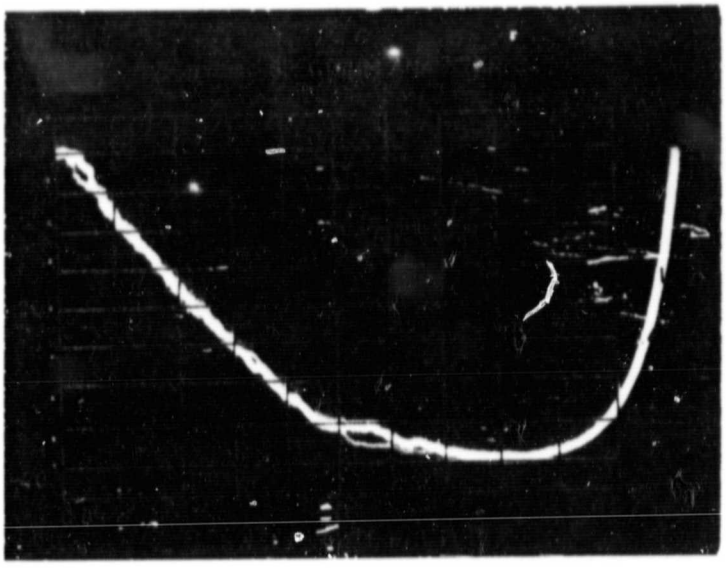

Figure 39. (Location 5c)

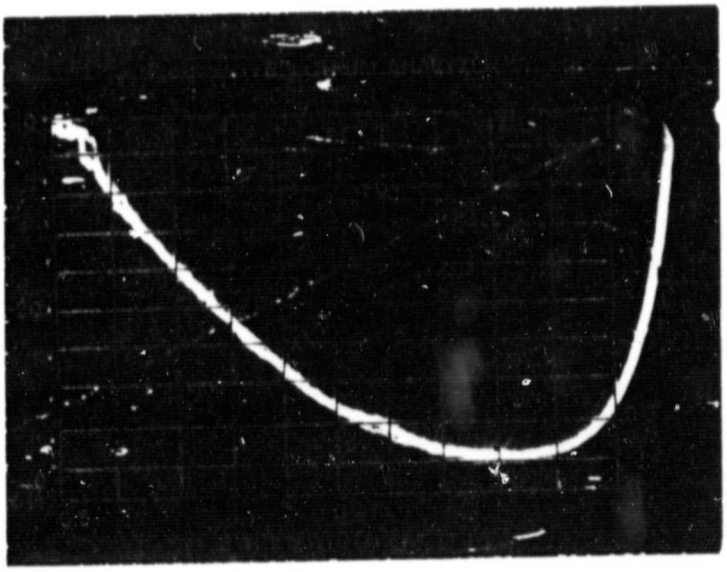

Figure 40. (Location 5d)

However the spectrum was quite unsteady and it appears that the transition from laminar to turbulent boundary layer takes place near this or just ahead of this station. Turbulence intensity beyond this station gradually increases and the spectrum becomes steady. From station (3) to station (4) there is a slight increase in the ratio of energy contained in larger eddies compared to smaller eddies. This increase in energy may be due to the extra rate of strain introduced by adverse pressure gradient along the surface of the airfoil and faster dissipation of smaller eddies.

Survey along points 'c' and 'd' did not show any marked variation in the energy spectrum. The turbulence intensity at station (1) is thought to be due to the stretching of the incoming vortex sheet. There is no variation in turbulence spectra along point 'd' because the boundary layer is already developed and the effect of the corner region is weak. Same is the case along point 'c' and the spectra remains the same as the free stream turbulence energy spectrum.

To maintain originality and accuracy of information, it is felt appropriate to retain the PFB units of System in the following Section of the Report which relates to wind tunnel design and construction.

5. DESIGN AND FABRICATION OF THE NEW WIND-TUNNEL

A low speed open circuit type wind tunnel design and its fabrication details are presented in this section. The main objectives for the present design were to obtain:

(I) A uniform velocity of 110 ft/sec in a test-section of 18 in. x 18 in.

(II) A turbulence level of the order of 0.25%

The free stream velocity of 110 ft/sec could be achieved at a flow rate of 14850 CFM (cubic feet per minute). The desired level of turbulence and uniformity in velocity distribution in the test-section could be achieved by appropriate choice of the combination of honeycomb and screens and by design of the settling chamber. An overall schematic diagram of the wind-tunnel is shown in Fig. 41. It consists of a centrifugal blower, divergent passage, constant area passage containing honeycomb and screens, a contraction passage and a test-section. The over-all wind-tunnel characteristics are presented in Table (3).

5.1 Overall Design Procedure

The design of the wind-tunnel comprised of two parts.

(I) Establishing the main dimensions of the tunnel

(II) Selection of honeycomb, screens, blower and motor

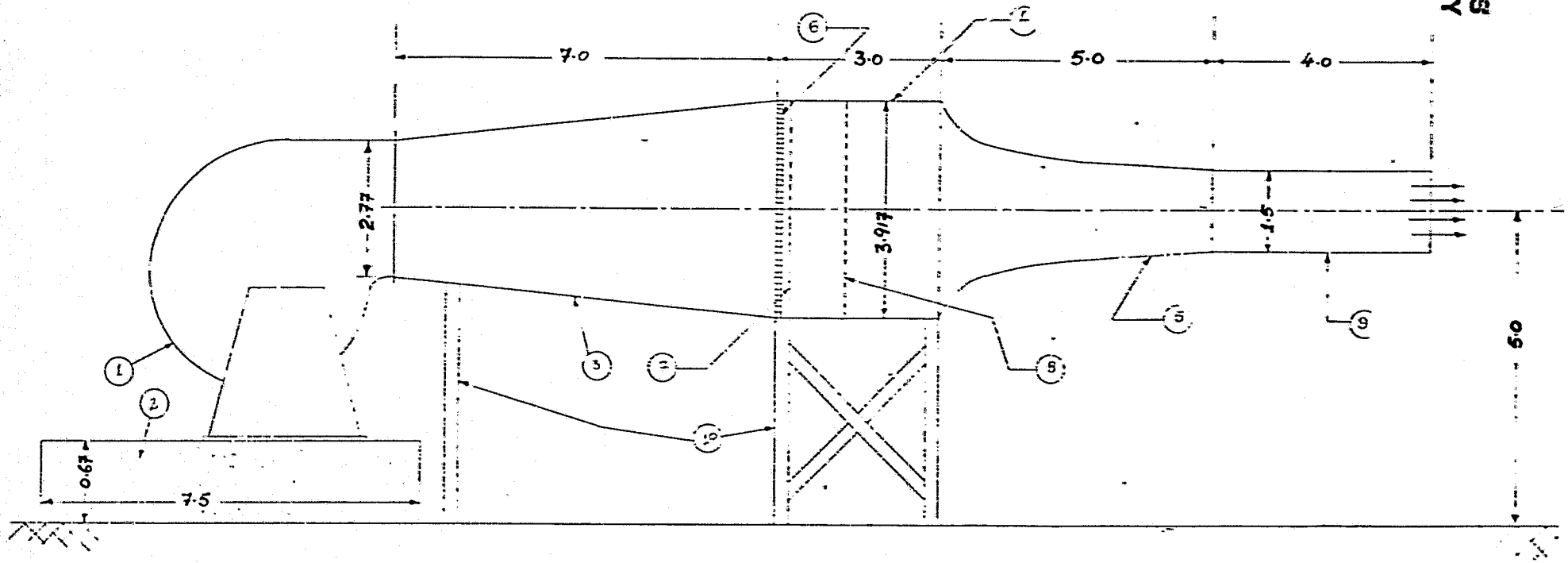

All Dimensions are in Feet.

Figure 41. New Wind Tunnel for Turbulence Measurements in Corner Flow

TABLE (3) - WIND - TUNNEL CHARACTERISTICS

S. No.	ITEM NAME	Part No. In Fig. 41	SPECIFICATION
1.	Air Supply Units	1	
1a	Motor		Motor HP-25, RPM-1800
1(b)	Fan		NEW YORK BLOWER Make Acousta Foil Fan, No.3 Class II with variable inlet damper for flow rate control, flow rate-16000 CFM, static pressure rise -6"WG, Outlet flow velocity-3600 ft/min.
2.	Concrete Foundation for Motor and Air Supply Unit	2	90" x 60" and height 8"
3.	Settling Chamber		
3(a)	Diverging Passage		Area ratio 2.97 and length is 7 ft.
3(b)	Constant Area Passage	4	Area of Cross-section 15.34 ft^2 Length 4 ft.
3(c)	Contraction Nozzle	5	Area ratio-6.82, Length 4 ft.
4.	Honeycomb & Screens		
4(a)	Honeycomb	6	Cell Size - 1/4 in. L/M = 8
4(b)	Screen No. 1	7	Mesh Size 10, width opening 0.075 in. Wire dia. - 0.025 in.
4(c)	Screen No. 2	8	Mesh Size-40, width of opening 0,015 in. Wire dia. - 0.010 in.
5.	Test Section	9	Cross-Section-18 in. x 18 in. free stream velocity - 110 ft/sec.
6.	Supporting Frame	10	Frame of wood for supporting tunnel

In establishing the major dimensions, the critical choice was the area of the plenum chamber which adjoins both the contraction and the diffusing passages. The consideration in this selection was to obtain low velocities (10 to 20 ft/sec) so that a minimum pressure loss occurs when the flow passes through the honeycomb and screens for a given velocity. The length of the diffuser part was selected to avoid separation. The length of plenum was selected to minimize turbulence and obtain a uniform flow. The length of the contraction part was based on the design of constant pressure drop across the contraction from plenum to test-section. To maintain symmetry, all cross-sections were made square. All the dimensional ratios in the design were kept within the limitations specified in the available literature.

The selection and location of screens in the plenum were to obtain a maximum possible uniformity in flow, low turbulence, and low pressure drop. The selection was made possible based on available literature, other wind-tunnel and design test data and specific studies made on honeycomb and grid turbulence. The selection of the blower was made to provide the required velocity in the test-section and generate enough static pressure to overcome all losses through the wind-tunnel. The blower selected had a variable inlet damper to control the velocity in the test section. A motor was selected based on power requirements to run the blower, overcome belt drive losses

and internal losses of the motor.

5.2 Component Design Calculations and Considerations in Design

5.2.1 Settling Chamber

5.2.1.1 Contraction Passage (Nozzle) - In the design of contraction passage, two important parameters are contraction ratio and length of the passage. A contraction ratio of 10-12 has been used in earlier wind-tunnel designs [83,84]. Wind-tunnel contraction reduces the turbulence level in the test-section. It has been shown that the absolute longitudinal fluctuations are reduced in a ratio lying between $1/\sqrt{n}$ and $2/\sqrt{n}$ where n is the contraction ratio [84]. The length of the contraction passage is selected such that the flow at exit stays uniform and the boundary layer developing on the walls of the passage stays thin. It is also pointed out in the literature that the effect of contraction is greatly dependent on the nature of the initial disturbance.

For the present design, a contraction ratio of 6.82 and length of 4 ft. was selected. The contraction ratio is well within the limits not to cause excess loss of pressure. The shape of the contraction passage is obtained by considering a constant pressure gradient at every section along the length of the passage. The cross-section is square at each section of the convergent passage. Since sudden contraction causes a large head loss, this loss can be reduced considerably

by employing a gradual contraction. It is shown that with a smoothly designed transition, a loss coefficient (k_c) of 0.05 is possible [85]. For conical reducers K_c of about 0.10 is obtained with cone angles between 20^o to 40^o. The head-loss due to contraction is evaluated by the use of relation given below.

$$h_c = k_c \quad U_4^2/2g_c$$

where k_c head loss coefficient. For the present calculation, a value of 0.10 is used.

U_4 - velocity at the exit end of contraction passage

Calculations for contraction passage and losses through it are presented below:

Applying continuity equation between section 3 and 4 and assuming incompressible flow we get,

$$U_3 = \frac{A_4}{A_3} \quad U_4$$

The contraction ratio (A_3/A_4) based on available literature [83,84] is chosen to be 6.82 and hence, A_3 = 15.34 ft^2 and U_3 = 16.13 ft/sec. The value of static pressure at section 3 is obtained using Bernoulli's equation.

$$P_3 + \frac{U_3^2}{2g_c} = P_4 + \frac{U_4^2}{2g_c}$$

and was found to be (P_3) = 2130.30 lbf/ft^2. The contraction passage shape is designed from consideration of constant pressure gradient at every section of the passage. From one-dimensional equation of motion for

inviscid and incompressible flow.

$$U \frac{dU}{dx} = -\frac{1}{\rho} \frac{dp}{dx}$$

The velocity at different sections of the nozzle and hence area of cross-section can be calculated by using the continuity equation. Length of contraction passage is taken to be 4 ft.

Pressure at inlet of contraction passage (p_3) = 2130.31 lbf/ft^2

Pressure at exit of contraction passage (p_4) = 2116.80 lbf/ft^2

Pressure drop per unit length $\frac{(dp)}{dx}$ = −3.38 lbf/ft^2

(Because total length of the contraction passage is 4 ft.)

Value of $-\frac{1}{\rho} \frac{dp}{dx}$ for the segment considered (length of each segment is 0.125 ft.) is = 185.09 ft^2/sec.^{2}

and $U \frac{dU}{dx}$ for the segment considered (= $U \frac{dU}{dx} dx$) = $\frac{dU^2}{2}$

Therefore, velocity at any section is given by the relation

$$\int_3^4 \frac{dU^2}{2} = \frac{U_4^2 - U_3^2}{2} = 185.09, \text{ or } U_4^2 - U_3^2 = 370.18, \text{ or}$$

$$U_4 = \sqrt{U_3^2 + 370.18}$$

The velocity and area calculations are presented in Table (4). The pressure loss in the contraction passage is calculated as follows:

The head loss in contraction passage is evaluated by using the relation,

$$h_c = k_c \frac{U_4^2}{2g_c}$$

TABLE 4

S. No.	Section (Ft)	Velocity (Ft/sec)	Area (Ft^2)	Height (Ft)
1	Inlet	16.13	15.34	3.92
2	0.125	25.11	9.85	3.14
3	0.250	31.63	7.82	2.80
4	0.375	37.02	6.68	2.58
5	0.500	41.72	5.93	2.43
6	0.625	45.95	5.38	2.32
7	0.750	49.81	4.97	2.23
8	0.875	53.40	4.63	2.15
9	1.000	56.76	4.36	2.09
10	1.125	59.93	4.13	2.03
11	1.250	62.94	3.93	1.98
12	1.375	65.82	3.76	1.94
13	1.500	68.57	3.61	1.90
14	1.625	71.22	3.47	1.86
15	1.750	73.77	3.35	1.83
16	1.875	76.24	3.24	1.80
17	2.000	78.63	3.15	1.77
18	2.125	80.95	3.06	1.75
19	2.250	83.21	2.97	1.72
20	2.375	85.40	2.90	1.70
21	2.500	87.54	2.83	1.68
22	2.625	89.63	2.76	1.66
23	2.750	91.67	2.70	1.64
24	2.875	93.67	2.64	1.62
25	3,000	95.63	2.59	1.61
26	3.125	97.54	2.54	1.59
27	3.250	99.42	2.49	1.58
28	3.375	101.27	2.44	1.56
29	3.500	103.08	2.40	1.55
30	3.625	104.86	2.36	1.54
31	3.750	106.61	2.32	1.52
32	3.875	108.33	2.28	1.51
33	Exit	110.00	2.25	1.50

Where k_c - head loss coefficient for gradual contraction = 0.10

U_4 - velocity at exit of contraction passage = 110 ft/sec

The value of h_c was found to be 0.27 inch WG (p in lbf/ft^2 = 1.405 lbf/ft^2)

5.2.1.2 Constant area passage (Plenum) - Wind tunnels in which air is supplied by a centrifugal fan have flow at the fan exit highly swirling and non-uniform. In addition the flow velocity is quite high. To reduce flow non-uniformities and turbulence level, a constant area passage with honeycomb and screens is employed downstream of the fan after a diverging passage. Some of the earlier wind-tunnels used only screens as a flow control device. Lumley [86] reported that for the same pressure drop honeycomb is more efficient in reducing turbulence intensity than screens. It is quite evident from the results [87] that pressure loss coefficient is larger if the length (L) of the honeycomb is increased for the same cell-size (M). A honeycomb of $L/M<10$ has been mentioned in the literature as suitable for wind-tunnels [83,87]. It has also been observed that the location of the peak of turbulence intensity moves downstream as the length of the honeycomb increases. But when a honeycomb is combined with a screen or screens, the effect of length of the honeycomb on turbulence peak displacement reduces. Moreover, a honeycomb-screen combination produces a much lower turbulence level than a honeycomb alone. This is because of the fact that the large scale jets exiting from the honeycomb cells are broken up into smaller scale eddies which decay faster. Distance between honeycomb and screen is critical to get a significant effect of the honeycomb-screen combination.

This distance has been reported to be less than 5M [87]. In the present design a honeycomb of 1/4 inch cell size and L/M = 8 is used (i.e. length of honeycomb cell, L is 2 inch). The distance of one inch (i.e. 4M cell size of honeycomb) is kept between honeycomb and first screen. A coarser screen is provided just after the honeycomb [88]. A screen of mesh size 10 is placed at a distance of one inch from the honeycomb. Similarly the full effect of multiple screens will be observed if they are placed far enough apart for the turbulence in the wire wakes of one screen to decay before the next screen is reached [83]. It is found that the distance between two screens should be at least 500 d (d is diameterof first screen). In the present wind-tunnel design, two screens are provided in the plenum chamber. Their mesh sizes are 10 and 40. Also from the data available [84], it is evident that the pressure loss is more for a screen of larger mesh size or, in other words, when the screen is of finer mesh. The details on flow control devices are given in Table (5). The calculations for the flow parameter and the pressure loss through the plenum chamber is as follows:
Flow conditions known at the exit of constant area passage (section-3) are:

$$P_3 = 2130.31 \text{ lbf/ft}^2,\ U_3 = 16.13 \text{ ft/sec},\ A_3 = 15.34 \text{ ft}^2,$$
$$\rho = 0.0735 \text{ lbm/ft}^3$$

TABLE 5

Screen Number	Mesh	Pressure Loss Coefficient, K	Wire Dia. (Inch)	Width of Opening (Inch)
1	10	1.4	0.025	0.075
2	40	5.0	0.010	0.0150

The flow irregularities are reduced by employing devices like screens and honeycomb. In order to estimate flow parameters at inlet of plenum chamber, the following procedure is adopted

(i) Losses are calculated through honeycomb and screens

(ii) Length of the constant area passage (plenum chamber) is decided based on the fact that the length must be sufficient for the decay of turbulence produced by the last screen.

(iii) Skin friction losses are calculated for the plenum chamber. For the calculation of skin friction losses, flow is considered turbulent in the plenum chamber.

Honeycomb selected has the following characteristics:
Cell size: 0.25", L/M ratio for honeycomb is 8, where L is the length of each cell in the direction of flow. In the present case, the length of honeycomb cell is 2". The pressure loss coefficient for honeycomb, k_h = 0.5 [87].

It was decided to use two screens and their important characteristics are given in Table (5). The values of pressure loss coefficients are calculated for free-stream velocity of 16.13 ft/sec (reference 84, Fig. 371). Values of wire diameter and width of opening are taken from Suppliers Bulletin; 5-10-a, Sherwatt Wire Cloth Co. Inc. [89]. Thus, total pressure loss coefficient due to honeycomb and two screens is $K_t = K_h + K_{s1} + K_{s2}$. Where, k_h - pressure loss coefficient of honeycomb, K_{s1} pressure loss coefficient of screen number 1, K_{s2} - pressure loss

coefficient of screen number 2 and was found to be 6.9. Since

$$K_T = \frac{\Delta p}{U^2/2g_c}.$$

Where U is the free stream velocity in the plenum chamber, the pressure drop due to these devices can be calculated using the above relation.

$$\Delta p = \frac{\rho U^2 K_T}{2g_c} = 2.05 \text{ lbf/ft}^2$$

The position of the first screen is determined, based on the earlier discussion, so that the distance between honeycomb and screen is less than 5 cell-size of honeycomb. Therefore, the screen No. 1 is placed at a distance of 1" from honeycomb end. This distance is 4 cell-size of honeycomb (honeycomb cell size is 0.25"). The distance between screen No. 1 and screen No. 2 is taken 500 wire diameter of first screen. This distance is therefore 12.5". Based on similar criteria of 500 diameter for screen No. 2, the distance required downstream is 5". The length of the total plenum chamber is taken as 4 ft.

The pressure loss in the plenum chamber is calculated as follows:

The calculations are based on flow through ducts. The pressure drop is calculated by using the relation,

$$\frac{\Delta p}{U^2/2g_c} = \frac{fL}{D_h} + K_L, \text{ where } K_L \text{ is the correction factor}$$

to take into account entrance effects, f is the friction factor,

D_h is hydraulic diameter. Value of D_h is 3.92 ft and K_L = 1.55, f Re_{D_h} = 56.91 [90]. Reynolds number based on hydraulic diameter is 37.46 X 10^4. Since the length of duct in the present case is small and flow is not fully developed, value of K_L is used to calculate pressure drop. Value of pressure drop (Δp) is 0.46 lbf/ft^2 (0.088" WG).

5.2.1.3 Diverging Passage (Diffuser): The divergent passage downstream of the fan is required to reduce flow velocities from the fan exit. In the present case, the fan exit velocity is of the order of 50 ft/sec. The flow at the fan exit is swirling and may have non-uniformities. To reduce the pressure losses, it is important to reduce flow velocity in the plenum chamber where flow control devices are used. For the present design, a velocity of the order of 16 ft/sec in the plenum chamber is within the specified range [84]. For the design of the divergent passage, important geometrical parameters are area ratio, A_2/A_1, and the axial length of the diffuser. Performance of the diffuser is also influenced by the inlet flow conditions. In such passages, the total pressure loss may be considered in two parts - one is the friction loss and the second is a turbulence loss set up by induced currents which produce a vortex motion over and above that which normally exists. Frictional losses will increase with the length of the diffuser. Length can be reduced for a given area ratio by increasing the angle of divergence. On the

other hand, turbulence losses will increase with increase of divergence and if this rate of divergence is large enough there may be a separation at the walls and eddies flowing backward along the walls. The total loss is the sum of the foregoing two losses. Optimum angle of divergence has been found to be 7^{o} [85,91,92]. A compromise is made in selecting the geometrical parameter. In wind-tunnel practice,a maximum area ratio of 5 has been used in the earlier design [83]. The area ratio for the present design is 2.97, to assure no separation over the chosen length. Axial length of the diffuser is 7 ft. Losses due to gradual expansion are evaluated by the use of relation:

$$h_d = \frac{K_d (U_1 - U_2)^2}{2g_c}$$

Where K_d is the pressure loss coefficient and its value is taken to be 0.2 [85], U_1 flow velocity at inlet of the diffuser, U_2 flow velocity at exit of the diffuser.

The calculation for the diverging passage and the pressure loss through it are as follows:

The area ratio selected for the present design, A_2/A_1 is 2.97 and therefore A_1 is 5.17 ft^2. This is the fan exit area (fan is available with exit area of 5.17 ft^2) or inlet area of cross-section of diverging passage. The performance

of the diffuser is influenced by the inlet flow conditions and is measured in terms of parameters like pressure recovery C_p, effectivenss C_p/C_{p_i} (C_{p_i} is ideal pressure recovery) and head loss. A compromise has to be made in the selection of diffuser geometry. As pointed out by Kline, et al and others [91,92], the optimum diffuser efficiency occurs when the included angle 2θ is about 7^o. At constant L_1/L_2, maximum recovery occurs at larger area ratios than maximum effectiveness (see Fig. 42 for notations). But minimum head loss occurs at lower area ratios than either maximum effectiveness or recovery. If the included angle is small, the length of diffuser becomes very large. In the present design as L_2 is fixed, in order to avoid large axial length L_1/L_2, should be small. L_1 in the present design has been selected to be 7 ft. Based on the value of L_1, values of θ are calculated for both the dimensions of inlet. Corresponding to fan exit dimensions (diffuser inlet dimensions) values of θ and L/L_2 are as follows:

(i) L_2 = 33.26 inch (2.77 Ft.), $\theta = 4.67^o$, $L/L_2 = 2.53$

(ii) L_2 = 22.385 inch (1,865 ft), $\theta = 8.33^o$, $L/L_2 = 3.79$

If we look into a typical performance chart for two-dimensional diffuser of such geometry, the diffuser efficiency is below 85% [91]. Now applying continuity between sections 1 and 2 (Fig. 4 2) we get

Figure 42. Notations for Diffuser Calculations

$U_1 = \frac{A_2}{A_1}$ U_2 = 47.91 ft/sec. From the definition of diffuser efficiency

$$\eta_d = \frac{2\,(P_2-P_1)}{\rho(U_1^2 - U_2^2)/g_c} \quad \text{or} \quad P_2-P_1 = \frac{\rho(U_1^2 - U_2^2)}{2\,g_c}\,\eta_d = 1.85 \text{ lbf/ft}^2$$

Therefore P_1 = 2130.50 lbf/ft^2

The head loss in the divergent passage is evaluated by using the relation.

$$h_d = \frac{k_d\,(U_1 - U_2)^2}{2\,g_c}$$, where k_d pressure loss coefficient and is chosen to be 0.2, U_1 flow velocity at inlet of diffuser = 47.91 ft/sec and U_2 flow velocity at exit of diffuser = 16.13 ft/sec.

Therefore h_d = 0.21 lbf/ft^2

5.2.2 Blower Requirement and Selection

Air is supplied to the wind-tunnel by an Acoustifoil fan, 309 SWSI (Single width, single inlet), Class II with maximum flow rate of 16000 ft^3/min. at a pressure rise of 6 inch WG (Water Gage) and 1600 RPM (revolution per minute). This centrifugal fan, manufactured and supplied by the New York Blower Company of Willowbrook, Illinois, is belt-driven (4 V-belts, BX-85-430 size) and powered with an A.C. motor of 25 H.P. with maximum speed of 1800 RPM. The flow rate is controlled with the help of an inlet damper, the setting of

which is controlled with a sophisticated electrically operated actuator. The inlet damper can be operated from fully open to fully closed position. Damper actuator RCS-MAR-10 extended duty with model No. 33-4 controller, modulating feed-back potentiometer is manufactured by Raymond Control Systems and supplied by New York Blower Company. Operationally this unit is very simple and requires a regulating switch which adjusts current through modulating feed-back potentiometer (4-20 milliamperes). Milliamperes readings are calibrated with damper angular settings and thus required flow rate can be obtained.

Calculations for the pressure rise through fan are as follows:

The static pressure rise through fan required is ΔP = 13.7 lbf/ft^2 (2.64 inch of water column).

Volume flow rate = test section area x maximum free stream velocity and is 14850 ft^3/min.

One fine screen is provided at the suction end of the fan to prevent any foreign material from being sucked into the wind-tunnel through the fan. For this, a pressure drop of 1" equivalent is taken into consideration (this is equal to 5.20 lbf/ft^2). Pressure rise required after considering various losses in different components is 20.975 lbf/ft^2 (4.04 in WG). where, pressure loss through contraction passage is 1.405 lbf/ft^2, pressure loss through constant area passage is 0.46 lbf/ft^2 and pressure loss through diverging passage is 0.21 lbf/ft^2.

5.2.3 Motor Requirements and Selection:

To estimate power requirement for the wind-tunnel, the following procedure is adopted.

From the known flow parameters at test-section, calculations are made to evaluate the value of pressure required at the fan exit. Losses occurring in various components of the wind-tunnel are taken into account. Pressure losses through flow control devices, honeycomb and screens, are also evaluated and taken into account. Based on these calculations a suitable motor is selected. Motor selected is an A.C. motor of 25 HP with maximum speed of 1800 RPM and is supplied by the New York Blower Company. The motor, manufactured by Westinghouse Electric Company, is 3 Phase, 60 cycles, 200 volts and 75 amperes and TEFC Type (totally enclosed fan cooled). Motor is provided with rail (frame No. 284T) for desired movement of the motor during assembly with the fan. An A.C. starter manufactured by Allen Bradley, No. 509 DAH-1, series A, Size 3, NEMA-1 enclosure, 3-Phase with overload heaters and built-in start and stop push button, is employed for the control of the motor. An additional general duty safety switch manufactured by Square D Company is used as a safety measure.

Calculations for the motor power are as follows:

The static pressure rise required is 18.90 lb/ft^2 (excluding the losses through various components). Power required to obtain this static pressure rise (Δp x volume flow

rate) = 8.505 HP. Also we note that the blower has to increase the kinetic energy of the air in addition to raising static pressure of the air. Power required to increase the kinetic energy (mass flow rate x 1/2 U^2) = 1.18 HP, where U is the velocity at fan exit. Thus the total power required by fan is 9.685 HP. Power of the motor is calculated considering efficiency of the blower and mechanical efficiency. For approximate evaluation purposes, efficiency of the blower is assumed 75% and mechanical efficiency to be 85%. Therefore power of the motor is 15.19 HP. In addition, the pressure drop due to friction losses in various components of the tunnel has to be considered. Additional power required to overcome these losses is 0.93 HP. Thus the total power required is 16.12 HP.

5.3 Fabrication Details

The fabrication of the tunnel required day to day supervision and it was not found feasible to subcontract its fabrication to outside contractors. Therefore all the fabrication work was done in the CCNY's Mechanical Engineering Department workshop.

5.5.1 Diverging passage. This passage of the wind-tunnel is constructed out of the 1/2" thick plywood sheets with one side very smooth. As the axial length of diverging passage is large (7 ft), the passage is strengthened by fixing additional support along the height, at a suitable position, made of 1-1/2" x 3-1/2" wooden slats. Sharp corners formed

at the joints in the passage were smoothed by placing cove molds of 1-5/8" all along the length of the passage. These molds are first glued with contact cement and subsequently nailed (size of nails used is one inch). Additional care was taken so that these molds are properly placed in the corner and no gap is left. Both the ends of the cove mold (wooden) are closed by using wooden plastic. To prevent any air leakage through the joints of the duct, contact cement is applied at the joining surfaces before final fixing with nails. Care is taken to prevent leakage through the joints by providing a fibre glass coating all along the length and for this purpose 2" wide fibre cloth ribbon is coated with resin. Flanges at both ends of the diverging passage are made with 1-1/2" x 3-1/2" wooden flats. Proper cutting of sides of flanges was necessary since the walls of diverging passage are at an angle.

5.5.2 Plenum Chamber (Constant Area Passage)

This part of the wind-tunnel is made in thee parts. Two passages are of 1 ft. length each and third one is of 2 ft. length. This was necessary so as to fix flow control devices such as honeycomb and screens at proper distances. The distance between these devices is very important in controlling the turbulence and non-uniformity as has been described in the previous sections. Honeycomb was cut 1/16" larger in size

as compared to the passage size in which it is fixed and then press fit into the passage. Cove molds are fitted in the corners of this duct in such a way so as to prevent any movement of the honeycomb. In this way, the honeycomb is properly positioned in the duct without any movement in axial direction. Flanges for this duct are made out of 1-1/2" x 3-1/2" wooden flats and are glued with contact cement before final fixing to the duct with nails of (M.S. nails). All the parts of constant area passage are made out of 1/2" thick plywood sheet with one side smooth. Screens are cut in larger than the duct opening (47" x 47") and are stapled in the flanges with the help of a special staple machine used in wood work. While installing the screens, special precautions were taken so as to avoid any sagging. Flanges for other plenum chamber ducts were made in a similar way as for the first one used for fixing honeycomb. In all the three ducts sharp corners are fitted with cove molds and closed at the ends with plastic wood. Exact distances between flow control devices are maintained by making the 3 ducts of suitable dimensions.

5.5.3 Nozzle (Convergent passage of the wind-tunnel): The most complicated part in the construction of the wind-tunnel was the fabrication of the converging passage. Many problems were experienced in its fabrication. Complications arose since the contracting passage required all the four walls of the nozzle to converge according to a complicated curve.

A number of materials were considered to construct this passage; sheet metal, plexi-glass, etc. Since we did not have proper facilities to make this part from sheet metal or plexi -glass we decided to fabricate this part out of flexible wooden sheets and later strengthen it with fibre glass. A long period of time was spent in finding suitable wooden sheets which could be bent in the desired contour. After a thorough survey in the market, we found suitable sheets called "Poplar sheets"which have sufficient flexibility. These sheets are 1/8" thick and were used in the fabrication of the nozzle. Four sheets were cut according to designed contours and then were slowly bent to the desired shape. In order to get the inner contour, a wooden mold was made. Rags soaked in water were spread outside of this structure in addition to fixing with plastic straps so that sheets took the desired shape. This was quite a slow process but the desired shape was finally obtained quite accurately. Firstly, all corners on the outer side were joined and fibre cloth ribbons were put on with a coating of resin. Polyester resin was used with suitable amount of hardener (1.5% by weight of resin - MEK peroxide in Dimethyl Phthalate) to achieve good structural strength. Once all the corners were properly assembled, the fibre glass sheets were laid to strengthen the nozzle structure. Suitable tools were used while working with fibre glass so that no air pockets between wooden surface and fibre cloth

are left. This way a good bonding was obtained. Final coating of resin was given to obtain a smooth surface. Inside the passage, all corners were fitted and smoothed by using special wooden putty.

Flanges at both ends of the converging passage are made out of 1-1/2" x 3-1/2" wooden flats. All parts of the settling chamber were assembled using 3/8" carriage bolts (3-1/2" long). Bolts were put 4" apart except at the ends of the flanges where the distance is 1-3/4" from the end because of joint considerations of flanges. Inner surface of all the parts of the settling chamber were given a number of coats of varnish (polyurethane clear high gloss variety) so as to achieve smooth surface. Gaskets (rubber) are provided in between each flange so as to prevent air leakage from the joints at the flanges. To support the wind-tunnel components a wooden frame was made out of 4" x 4" wooden flats and the frame was firmly bolted to the cemented floor. The photograph of wind-tunnel assembly is shown in Figure 43.

C-2

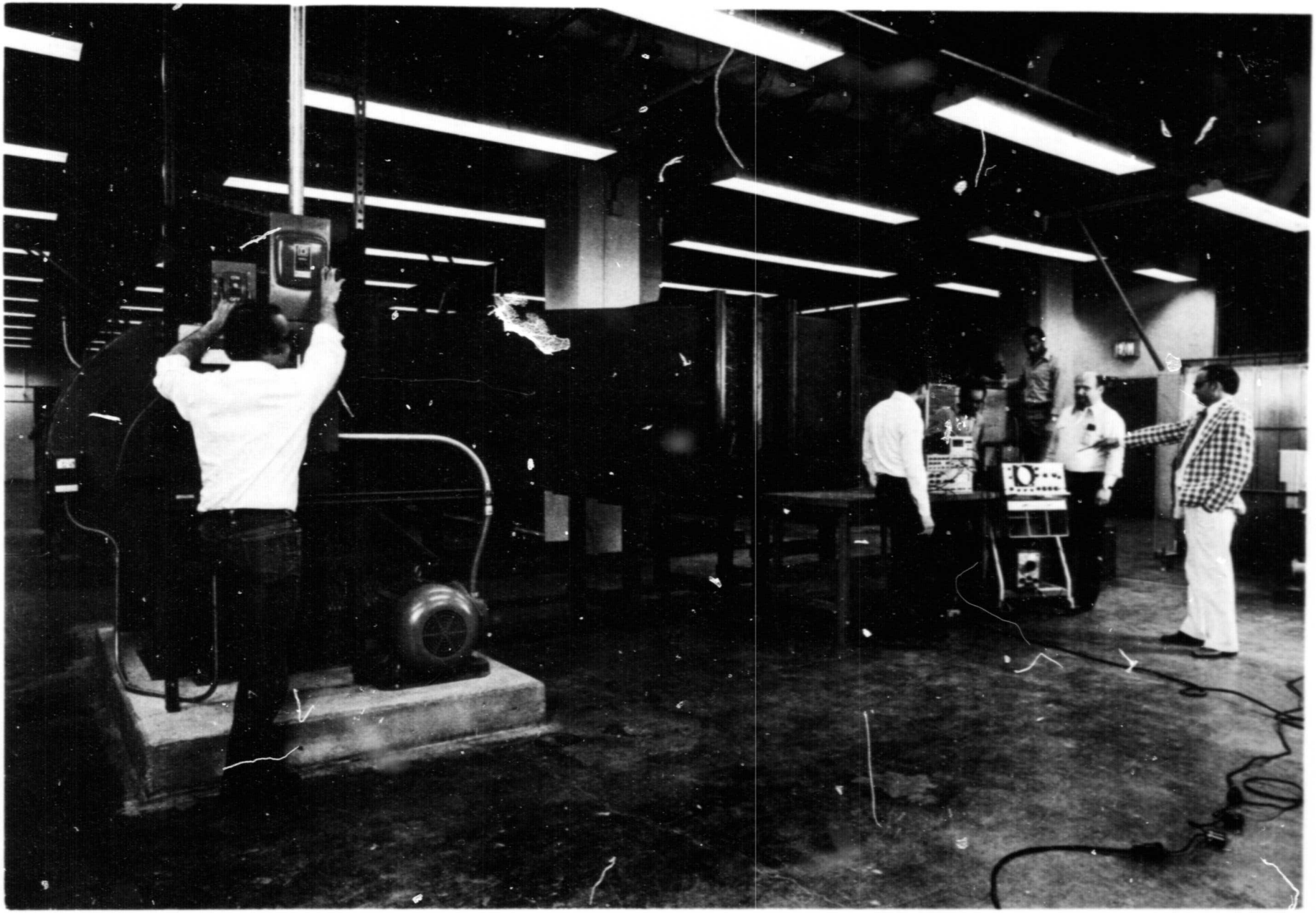

Figure 43. Photograph of Newly Built Wind-Tunnel

ACKNOWLEDGEMENTS

The day to day technical work on the project was conducted by the Principal Investigator and his two Doctoral students; Messrs. B. K. Hazarika and R.K. Bhargava. The fabrication of the wind tunnel facility was done by the Mechanical Engineering Department technicians; Messrs. G. Noll and B. Roiss. Help was also rendered by the undergraduate students; Messrs. A, Aprahamian and John Cessar of the Mechanical Engineering Department in the fabrication and assembly of the wind tunnel. Thanks are also expressed to Curtiss-Wright engineering Mr. W. Franklin for various suggestions made in the design of the wind tunnel facility.

LIST OF FIGURES

REFERENCES

1. Carrier, G.,
"The Boundary Layer in a Corner." Quart. of Appl. Math., 1947, Vol. 4, No. 4, P. 367.

2. Dowell, R.B.,
"Incompressible Boundary Layer Flow Along Interior Corners," Proceeding 10th Midwestern Conf. on Mechanics Colorado State University, Fort Collins, Aug. 1968, p. 1355.

3. Pearson, J.R.A.,
"Homogenous Turbulence and Laminar Viscous Flow," Ph. D. thesis, Cambridge U. , 1957.

4. Rubin, S.G.,
"Incompressible Flow Along a Corner," JFM, Vol.26, Part 1, 1966, p. 97.

5. Pal, A. and Rubin, S.G.,
"Asymptotic Features of the Viscous Flow Along a Corner," Quart. of Applied Math. Vol. 29, 1971, p. 91

6. Rubin, S.G. and Grossman, B.,
"Viscous Flow Along a Corner: Numerical Solution of the Corner Layer Equations," Quart. of Applied Math. Vol. 29, No. 2, 1971, p. 169.

7. Zamir, M.,
"Bounary Layer Theory and the Flow in a Streamwise Corner," Aeron. J. of the R.A.C., Vol. 74, 1970, p. 330.

8. Zamir, M.,
"On the Corner Boundary Layer with Favourable Pressure Gradient," Aero.Quarterly, Vol. 23, 1972, p. 161.

9. Zamir, M.,
"Further Solution of the Corner Boundary Layer Equations," Aero. Quart. Vol. 26, 1973, p. 219.

10. Ghia, K.N. and Davies, R.T.,
"A Study of Compressible Potential and Asymptotic Viscous Flows for Corner Region," A.I.A.A. Journal,Vol. 12, 1974, p. 355.

11. Ghia, K.N.,
"Streamwise Flow Along an Unbounded Corner," A.I.A.A. Journal, Vol. 13, No. 7, 1975, p. 902.

12. Patel, D.K. and Goglia, G. L.,
"Investigation of an Incompressible Flow Along a Corner by and Alternating Direction Implict Method," N.A.S.A. - CR - 154648, N17 - 30409, 1977.

13. Zamir, M. and Young, A.D.,
"Experimental Investigation of the Boundary Layer in a Streamwise Corner," Aeron. Quartarly, Vol. 21, 1970, p. 313.

14. Barclay, W.H.,
"Laminar Flow in a Streamwise Corner," Ph.D. thesis, University of London, 1971.

15. Barclay, W.H.,
"Experimantal Investigation of the Laminar Flow Along a Straight 135° Corner," Aero. Quart., 1973, Vol. 24, p. 147.

16. El-Gamal, H.A.,
"Laminar Flow Along a Corner with Boundary Layer Suction," Ph. D. thesis, U. of London, 1977.

17. El-Gamal, H.A. and Barclay, W.H.,
"Experiments on the Laminar Flow in a Rectangular Streamwise Corner," Aero. Quart., 1978, Vol. 29, Part 2, p. 75.

18. Ligget, J.A., Chiu, C.L. and Miao, L.S.,
"Secondary Currents in a Corner," J. of Hydraulics Div., Proc., A.S.C.E., Vol. 91, 1965, p. 99.

19. Toan, N.K.,
"Application of Integral Methods to the Turbulent Corner Flow Problem," A.S.M.E. Paper No. 71 - WA/FE36, 1971.

20. Bragg, G.M.,
"The Turbulent Boundary Layer in a Corner,"Ph.D. thesis, University of Cambridge, 1965.

21. Bragg, G.M.,
"The Turbulent Boundary Layer in a Corner," J.F.M. 1969, Vol. 36, p. 485.

22. Gersten, K.,
"Corner Interference Effects," AGARD Report 299, 1959.

23. Perkin, H.J.,
"The Formation of Streamwise Vorticity in Turbulent Flow," J.F.M., Vol. 44, Part 4, 1970, p. 721.

24. Ibragimore,M.K., Petrischchere,V.S. and Sabelere, G.I.,
"Calculation of Secondary Flow in a Turbulent Fluid Stream," Fluid Dynamics , Vol. 4, No. 4, 1969, p. 114.

25. Gerard, R.,
"Turbulent Flow in Non-Circular Conduits," Ph.D. thesis, University of New Castle, New South Wales, Australia, 1970.

26. Klinbeik, D.,
"An Implicit Numerical Solution for the Axis of a 90° Corner," Ph.D. thesis, M.E. Dept., Virgina Polytech. Instt. and State U., 1972.

27. Launder, B.E., and Ying, W.M.,
"Prediction of Flow and Heat Transfer in Ducts of Square Cross Section," Heat and Fluid Flow, Vol. 3, 1973, p. 115.

28. Gessner, F.B., and Emery, A.F.,
"A Reynolds Stress Model for Turbulent Corner Flows - Part I: Development of the Model," J of Fluids Engineering, Trans, A.S.M.E., Series I, Vol. 98, 1976, p. 261.

29. Gessner, F.B., and Emery, A.F.,
"A Length Scale Model for Developing Turbulent Flow in a Rectangular Duct," J. of Fluids Engineering Trans. A.S.M.E., Series I, Vol. 99, 1977, p.347.

30. Gessner, F.B., and Pu, J.K.,
"A Reynolds Stress Model for Turbulent Flows - Part II: Comparisons Between Theory and Experiment," J. of Fluids Engg., Trans. A.S.M.E., Series I, Vol. 98, 1976, p. 269.

31. Nact, D., Shavit, A. and Wolfstein, M.,
"Numerical Calculation of Reynolds Stress in a Square Duct with Secondary Flow," Warme und Stoffubertragung, Vol. 7, No. 3, 1974, p. 151.

32. Tatchell, D.G.,
"Convection Process in Confined Three-Dimensional Boundary Layers," Ph.D. thesis, U. of London, 1975.

33. Mikhail, A.G. and Ghia, K.N.,
"Analysis and Asymptotic Solutions of Compressible Turbulent Corner Flow," A.S.M.E. Paper No. 81-GT-149, 1981.

34. Cebeci, T.,
"Calculation of Three-Dimensional Boundary Layers: II, Three-Dimensional Flows in Cartesian Coordinates," A.I.A.A. Journal, Vol. 13, No. 8, Aug. 1976, p. 1056.

35. Shafir, M. and Rubin, S.G.,
"The Turbulent Boundary Layer Near a Corner," A.S.M.E. J. of Applied Mechanics, Dec. 1976, p. 567.

36. Rodet, E.,
"Etude de L'ecoulement d'un flude dans un tunnel prinatique de section trapezoidale," Publications Scientifiques et Techniques du Ministre de l'Air, No. 369, 1960.

37. Brundrett, E.,
"The Production and Diffusion of Vorticity in Channel Flow," Ph.D. thesis, University of Toronto, 1963.

38. Gessner, F.B. and Jones, J.B.,
"A Preliminary Study of Turbulence Characteristics of Flow Along a Corner," A.S.M.E. J. of Basic Engineering, Vol. 83, 1961, p. 657.

39. Leutheusser, H.J.,
"Turbulent Flow in Rectangular Ducts," J. of Hydraulics Division, Proc. A.S.C.E., Vol. 89, 1963, p.1.

40. Ahmed, S. and Brundrett, E.,
"Turbulent Flow in Non-Circular Ducts Mean Flow Properties in the Developing Region of a Square Duct," Int. J. Heat and Mass Transfer, 1977, Vol. 14, p. 365.

41. Mojola, O.O. and Young, A,D.,
"An Experimental Investigation of Turbulent Shear Flows," AGARD Cong. Proc. (C p-93), 1971 p. 121.

42. Mojola, O.O.,
"Turbulent Boundary Layer Along a Streamwise Corner," Ph.D. thesis, U. of London, 1972.

43. Herzig, H.Z., Hansen, A.G. and Castello, G.R.,
"A visualization Study of Secondary Flows in Cascades," NACA Report 1163, 1953.

44. Armstrong, W.D.,
"The Secondary Flow in a Cascade of Turbine Blades," ARC Reports & Memoranda No. 2979, 1955.

45. Armstrong, W.D.,
"An Experimental Investigation of the Secondary Flow Occuring in a Compressor Cascade," Aero. Quart., 1957, Vol. 8, p. 240.

46. Turner, J.R.,
"An Investigation of the Endwall Boundary Layer of a Turbine Nozzle Cascade," Trans. A.S.M.E., Vol. 19, 1957, p. 1801.

47. Senoo, Y.,
"Three-Dimensional Laminar Boundary Layer in Curved Channel with Acceleration," Trans. A.S.M.E., Vol. 80, 1958, p. 1721.

48. Came, P.M.,
"Secondary Loss Measurements in a Cascade of Turbine Blades," Inttn. Mechhanical Engineers, Conference Pub. 3, 1973, p. 75.

49. Carrick, H.B.,
"Preliminary Experimental Results on the Effect of Skew in the Boundary Layer on the Secondary Flow in an Impluse Turbine Cascade," ARC 35915, Turbo. 352, 1975.

50. Prumper, H.,
"Methoden Zur Verminderung der Sekundarverticste in Axialen Turbinenstufer," Zeitschrift fur Flugwissenschafter, 20, 1972, p. 60.

51. Belik, L.,
"Secondary Flow in Blade Cascades of Axial Turbomachines and Possibility of Reducing its Unfavourable Effects," Second Intl. J.S.M.E. Symposium, Fluid Machinery and Fluids, Tokyo, September 1972, p. 41.

52. Owezarek, J.A. and Rockwell, D.O.,
"An Experimental Study of Flow in Planar Nozzle," Trans. A.S.M.E. J. of Basic Engg.,Vol. 94, Series D, No. 3, p. 682.

53. Owezarek, J.A., Rockwell, D.O. and Cha, Y.S.,
"A Study of Flow from Two Planar Nozzle, " Leigh University Technical Report No. 1.

54. Dring, R.P.,
"A Momentum Integral Analysis of the Three-Dimensional Turbine Endwall Boundary Layer," J.E.P., Trans. A.S.M.E. Series Cm Vol. 93, 1971, p. 386.

55. Sjolander, S.A.,
"The End-Wall Boundary Layer in an Angular Cascade of Turbine Guide Vanes," Carleton University, Dept. of Mech. & Aerospace Engg., Ottowa, Canada, TR ME/A 75-4, 1975.

56. Langston, L.S., Nice, M.L. and Hooper, R.M.,
"Three-Dimensional Flow Within a Turbine Cascade Passage," J.E.P., Jan.1977, p. 21.

57. Bradshaw, P., Cebeci, T. and Whitelaw, J.H.,
"Engineering Calculation Methods for Turbulent Flows," Lecture Series, M.E. Dept., California State University, Long Beach, June 1977.

58. Marchal, P.H. and Sieverding, C.H.,
"Secondary Flows Within Turbomachinery Blading," AGARD C p-214 on Secondary Flows in Turbomachinery, No. 11, 1977.

59. Penken, J.H.,
"Corner Layer and Secondary Flow Within a Straight Compressor Cascade," Paper 21, AGARD-CP-214, On Secondary Flows in Turbomachines, 1977.

60. Lakshminarayan, B., Davino, R. and Pouagare, M., "Three-Dimensional Flow Field and Annulus Wall Boundary Layer Development in the Tip Region of a Compressor Rotor Passage," A.S.M.E. Gas Turbine Conference, London, 1982.

61. Lakshminarayan, B., Davino, R. and Pouagare, M., "Turbulence Properties in the Tip Region of Compressor Rotor Passage," (unpublished).

62. Vasant Ram, V., "Experimentelle Untersuchungen der Stromung entlang einer rechtiowinkligen Ecke Zwischen einen profil und edner ebenen Seitenwand," Institut fur Stromungmechanick, Technische Hochschule Braunschweig Bericht 63/17.

63. East, L.F. and Honey, R.P., "Boundary Layer Effect in an Idealized Wing-Body Junction at Low Speed," RAE Tech. Report TR68161, 1968.

64. East, L.F. and Honey, R.P., "Low Speed Three-Dimensional Turbulent Boundary Layer Data. Part 2," RAE Tech. Report TR69137, 1969.

65. Sepri, P., "An Investigation of the Flow in the Region of the Junction of a Wing and a Flat Surface Normal to the Wing Span," Queen Mary College, Departmental Report, QMC ER-1002.

66. Chu, J.K. and Young, A.D., "A Further Investigation of Viscous Effects in a Wing Plate Junction," Queen Mary College Departmental Report, E.R. 1003.

67. Young, A.D., "Some Special Boundary Layer Problems," Z. Flugwiss, Weltraumforsch 1, Heft 6, 1977, p. 401.

68. Naranjit, S., "An Investigation of Flow Over a Wing-Body Combination," Ph.D. thesis, Univ. of London, 1976.

69. Shabaka, I.M.M.A., "Turbulent Flow in an Idealized Wing-Body Junction," Ph.D. thesis, U. of London, 1979.

70. Murray, J.C.,
"Incompressible Flow Past a Wing-Body Combination Using General Curvilinear Coordinates," Aeron. Quartly, 1979 Vol. 30, p. 451.

71. Kraichnen, R.H.,
"Pressure Field within Homogenous Anisotropic Turbulence," J. Acoustical Soc. Am. Vol. 28, 64-72 (Jan. 1956).

72. Willmarth, W.W. and Wooldridge, C.E.,
"Measurements of the Fluctuation Pressure at the Wall beneath a Thick Turbulent Boundary Layer," J. Fluid Mech., Vol. 14, 187-210, (1962).

73. Bradshaw, P., and Koh, Y.M.,
"A Note on Poisson's Equation for Pressure in a Turbulent Flow," Phys. Fluid, Vol. 24, No. 4, April 1981, p. 777.

74. Corcos, G.M.,
"The Structure of the Turbulent Pressure Field in Boundary Layer Flows," J.F.M., Vol. 18, 1964, (353-378).

75. Uberoi, M.S.,
"Quadruple Velocity Correlations and Pressure Fluctuations in Isotropic Turbulence," J.Aero. Sci., Vol. 20, 1953, (197-204).

76. Willmarth, W.W., and Ross, F.W.,
"Resolution and Structure of the Wall Pressure Field beneath a Turbulent Boundary Layer," J. Fluid Mech., Vol. 22, 81-94 (1965).

77. Bull, M.K.,
"Wall-Pressure Fluctuations Associated with Subsonic Turbulent Boundary Layer Flow," J.F.M., Vol. 28, 719-754 (1967).

78. Blake, W.K.,
"Turbulent Boundary Layer Wall Pressure Fluctuations on Smooth and Rough Walls," J.F.M., Vol. 44, 637-660 (1970).

79. Wills, J.A.B.,
"Measurements of the Wave Number/Phase Velocity Spectrum of the Wall Pressure beneath a Turbulent Boundary Layer," J.F.M., Vol. 45, 65-90 (1970).

80. Kistler, A.L. and Chen, W.S., "The Fluctuating Pressure Field in a Supersonic Turbulent Boundary Layer," J.F.M., Vol. 16, 41-64 (1963).

81. Lotsch, H.K.V., "Pseudo Sound in a Plane, Turbulent Boundary Layer Flow," Report from Electro- Acoustical Sonar Systems 1971.

82. Corcos, G.M., "Resolution of Pressure in Turbulence," J. Acoustical Soc. Am., Vol. 35, No. 2, 192-199, (1963).

83. Bradshaw, P. and Pankhurst, R.C., "The Design of Low Speed Wind-Tunnels," Progress in Aeronautical Sciences, Vol. 5, MacMillan Company, 1964.

84. Pankhurst, R.C. and Holder, D.W., "Wind-Tunnel Technique - An Account of Experimental Methods in Low and High Speed Wind-Tunnels," Sir Isaac Pitman and Sons Ltd., 1968.

85. Daugherty, R. L. and Franzini, J. B., "Fluid Mechanics with Engineering Application," McGraw-Hill Book Company, 1977.

86. Lumley, J.L. and McMahon, J.F., "Reducing Water Tunnel Turbulence by Means of Honeycombs," Trans. ASME, Journal of Basic Engineering, Paper No. 67-FE-5, pp. 764-770 (1967).

87. Loehrke, R.I. and Nagib, H.M., "Control of Free-Stream Turbulence by Means of Honeycombs: A Balance Between Suppression and Generation," Trans. ASME, Paper No. 76-FE-2 (1976).

88. Blair, M.E. et al, "Development of a Large Scale Wind-Tunnel for the Simulation of Turbomachinery Airfoil Boundary Layers," Trans. ASME, Paper No. 81-GT-6 (1981).

89. Bulletin S-10-a, Sherwatt Wire Cloth Co., Inc., New York.

90. Olson, Reuben, M., "Essentials of Engineering Fluid Mechanics," Third Edition, Intext Educational Publishers, New York, 1973.

91. Dixon, S.L., "Fluid Mechanics and Thermodynamics of Turbomachinery, Third Edition, Pergamon Press, 1978.

92. Kline, S.J. et al, "Performance and Design of Straight, Two-Dimensional Diffusers," Trans. ASME Journal of Basic Engineering PP. 141-150 (1967).